JGR Planets

RESEARCH ARTICLE

10.1029/2021JE006974

Key Points:

- Geological evidence supporting a SE-NW facies change within intracrater layered deposits in western Arabia Terra
- Measurements of deposit thickness and individual layer thickness decrease with elevation and latitude
- The volume required to fill these craters in an air fall scenario is in opposition with the locations of known volcanic provinces and the volume of ash volcanic eruptions produce

Correspondence to:

G. Schmidt,
genewalter.schmidt@uniroma3.it

Citation:

Schmidt, G., Pondrelli, M., Salese, F., Rossi, A. P., Le Deit, L., Fueten, F., & Salvini, F. (2021). Depositional controls of the layered deposits of Arabia Terra, Mars: Hints from basin geometries and stratigraphic trends. *Journal of Geophysical Research: Planets*, *126*, e2021JE006974. https://doi.org/10.1029/2021JE006974

Received 8 JUN 2021
Accepted 15 SEP 2021

Author Contributions:

Conceptualization: G. Schmidt, M. Pondrelli, F. Salese
Data curation: G. Schmidt, M. Pondrelli, F. Salese, A.P. Rossi
Formal analysis: G. Schmidt, M. Pondrelli
Funding acquisition: M. Pondrelli
Investigation: G. Schmidt, M. Pondrelli
Methodology: G. Schmidt, A.P. Rossi, F. Fueten
Project Administration: M. Pondrelli
Resources: G. Schmidt, M. Pondrelli, F. Salese, A.P. Rossi
Software: F. Fueten

Depositional Controls of the Layered Deposits of Arabia Terra, Mars: Hints From Basin Geometries and Stratigraphic Trends

G. Schmidt[1], M. Pondrelli[2], F. Salese[2,3], A.P. Rossi[4], L. Le Deit[5], F. Fueten[6], and F. Salvini[1]

[1]Department of Science, Università Degli Studi Roma Tre, Rome, Italy, [2]International Research School of Planetary Sciences, Università d'Annunzio, Pescara, Italy, [3]Centro de Astrobiología (CSIC-INTA), Madrid, Spain, [4]Department of Earth and Planetary Science, Jacobs University Bremen, Bremen, Germany, [5]Laboratoire de Planétologie et Géodynamique, CNRS UMR, Université de Nantes, Université d'Angers, Nantes, France, [6]Department of Earth Sciences, Brock University, St. Catherines, ON, Canada

Abstract An extensive distribution of water-altered equatorial layered deposits (ELDs) characterizes the densely cratered terrain of Arabia Terra (AT), Mars. The majority of these deposits reside within craters and are easily identified by laterally continuous layering. The processes that led to their formation have been widely investigated, but remain unresolved. Furthermore, their precise spatial distribution as a whole, as well as their relationship to one another individually, has yet to be fully appreciated. This work examines 1,013 craters and emphasizes 45 that were observed to contain ELDs within the eastern half of AT. We present the statistical relationships between crater characteristics (e.g., location, diameter, depth), as well as evidence supporting a southeast-northwest facies change. The 30–2,000-m range of measured deposit thicknesses, accompanied with individual layer thicknesses, correlate with crater elevation either due to water level differences within craters, or a proximal-distal relationship to the source. Air fall or fluid expulsion appear to stand out among all the prevailing depositional hypotheses, however the volume required to fill these craters in an ash fall scenario is in opposition with the locations of known volcanic provinces and the volume of ash that volcanic eruptions produce. This new evidence of a regional facies change provides a unique opportunity to better understand past climate and sedimentary processes on Mars, as well as the putative groundwater level in ancient AT. Ultimately, our results do not agree well with a unified depositional method for these deposits and the possibility of mixed origins should be taken seriously.

Plain Language Summary Layer thicknesses of equatorial layered deposits (ELDs) within craters in western Arabia Terra (AT) show a regional NW-SE thickening, correlating with both elevation and latitude. The trend does not correlate with locations of established volcanic provinces or proposed locations of nearby calderas. Additionally, the volume necessary to completely fill craters may be problematic in an ash fall scenario. The discrepancy of ELD size between craters is problematic and requires specialized erosional intensities unique to each crater. Fluctuating water level might create a proximal-distal effect either from the putative ocean to the northwest which hinders thicker ELD formation, or fluid expulsion focused at Meridiani Planum which aids thicker ELD formation. Thinning and thickening sequences in individual craters suggests repeated changes from low to high energy environments. Low to moderate layer attitudes are indicative of compaction or draping during deposition over pre-existing topography, whereas steeply dipping layers suggests post-depositional deformation in specific craters. This implies post-depositional histories are often unique to individual craters. Observations demonstrate that determining the depositional method requires a regional overview to establish the controls that create these unique characteristics. Thus, a unifying depositional theory does not fit all characteristics of ELDs in AT and multiple or mixed origins should be considered.

1. Introduction

Mars has been famous for the presence and diversity of water-altered minerals since they were detected on the surface by the Mars Global Surveyor, Mars Express, and Mars Reconnaissance Orbiter missions (e.g.,

Supervision: M. Pondrelli, F. Salese, A.P. Rossi, L. Le Deit
Validation: G. Schmidt, M. Pondrelli, F. Salese, A.P. Rossi, L. Le Deit
Visualization: G. Schmidt, F. Salese
Writing – original draft: G. Schmidt
Writing – review & editing: G. Schmidt, M. Pondrelli, F. Salese, L. Le Deit, F. Fueten

Bibring et al., 2006; Carter et al., 2013; Christensen et al., 2001; Gendrin et al., 2005; Murchie et al., 2009).

Among the surface features most often associated with water-altered minerals are the layered mounds and deposits, which captured the attention of scientists to such an extent that one was ultimately selected as the landing site for the Mars Science Laboratory (MSL). The origins of equatorial layered deposits (ELDs), often called light-toned layered deposits (LTD/LLDs) (Ansan et al., 2011; Catling et al., 2006; Mangold, Carter, et al., 2012; Salese et al., 2016; Sarkar et al., 2018; Tanaka & Platz, 2011; Weitz et al., 2010) or ILDs (interior layered deposits) (Al-Samir et al., 2017; Fueten et al., 2008, 2010, 2014, 2017; Komatsu et al., 2004; Lucchitta et al., 1994; Michalski & Niles, 2012; Noel et al., 2015; Okubo et al., 2008; Schmidt et al., 2018; Sefton-Nash et al., 2012; Sowe et al., 2011), are a topic of ongoing debate and remain one of the most coveted areas of planetary research. We recognize that the terms ELD, ILD, LTD, and LLD are often used interchangeably. For example, the difference between an ELD within a depression and an ILD has not been made clear, aside from "ILD" being the preferred nomenclature for layered deposits in Valles Marineris despite they too being located in the equatorial region. For purposes of this study, layered deposits are referred to as ELDs, specifying layered deposits within the craters of Arabia Terra (AT) (Figure 1) and separating them from plateau deposits (Fergason & Christensen, 2008), while still recognizing that they both have similar chemical compositions and may share formation origins.

Although the composition, distribution, and post-depositional history (e.g., faulting, erosion, and alteration) of ELDs can be recognized, depositional processes remain difficult to determine (Annex & Lewis, 2020; Bennett & Bell, 2016; Cadieux & Kah, 2015; Day et al., 2019; Lewis & Haronson et al., 2014; Pondrelli et al., 2019, 2015; Zabrusky et al., 2012). ELDs are generally characterized by a high albedo relative to their surroundings, as well as by their laterally continuous layering (Annex & Lewis, 2020; Franchi et al., 2014; Lewis & Haronson et al., 2014; Pondrelli et al., 2019). ELDs formed within basins or craters tend to have significant volume, often filling the entire basin (Day et al., 2016; Franchi et al., 2014; Pondrelli et al., 2019). The need for more reliable methods to understand their distribution and formation processes, particularly at a regional scale, is vital to the future of Mars exploration. A variety of processes and depositional regimes, both sedimentary and volcanic, have been proposed to explain ELD formation and include lacustrine (Day et al., 2019; Lucchitta, 2010; Wharton et al., 1995; Wray et al., 2011), groundwater upwelling (Allen & Oehler, 2008; Andrews-Hanna et al., 2010; Franchi et al., 2014; Pondrelli et al., 2015, 2019; Rossi et al., 2008), ash fall (Fassett & Head, 2007; Fueten et al., 2014; Kerber et al., 2012; Le Deit et al., 2013; Schmidt et al., 2018), diapiric uplift (Jackson et al., 2011), dust rich glaciers (Bennett & Bell, 2016; Fergason & Christensen, 2008; Michalski & Niles, 2012), aeolian deposition (Annex & Lewis, 2020; Kite et al., 2016, 2013; Lewis & Aharonson et al., 2014; Hayes et al., 2011), and a combination of multiple processes (Bennett & Bell, 2016; Cadieux & Kah, 2015; Fueten et al., 2014; Le Deit et al., 2013; Schmidt et al., 2018; Zabrusky et al., 2012). These sedimentary deposits are widespread and their occurrence in AT was first identified by Malin and Edgett (2000). All proposed depositional methods have their own drawbacks, in that they can readily explain some features of the deposits while neglecting others. Regardless, the deposition and aqueous alteration of layered deposits is generally accepted to have spanned across the Late Noachian and Early Hesperian (Bibring et al., 2006; Carr & Head, 2010; Lowe et al., 2020; Poulet et al., 2008). Deposition is thought to have occurred in the beginning of the Hesperian (Bibring et al., 2006; Poulet et al., 2008), more specifically between ≈3.83 and 3.56 Ga (Zabrusky et al., 2012), and marked by a commonly proposed global change in Martian climate (Bibring et al., 2006; Carr & Head, 2010). Some deposition may have occurred as recently as the Amazonian as determined for the Medusae Fossae Formation (Mandt et al., 2008; Morgan et al., 2015; Neukum et al., 2010; Werner, 2005). However, age determination is inhibited by the extensive erosion of subset craters used for age dating (Hartmann, 2005) and ELDs have been characterized previously as having a very low crater retention age (Pondrelli et al., 2019).

2. Geological Setting

AT is a large regional dichotomy which represents the transition between the southern highlands and the northern lowlands (Evans et al., 2010; Smith et al., 2001; Zuber et al., 2000) (Figure 1). Well known for a high density of craters, many of which contain ELDs (Cadieux & Kah, 2015; Day et al., 2019; Franchi et al., 2014; Pondrelli et al., 2019; Zabrusky et al., 2012), AT represents a unique geologic story which combines the dynamics of sedimentary deposition, erosion, crustal dynamics, explosive volcanism, and groundwater

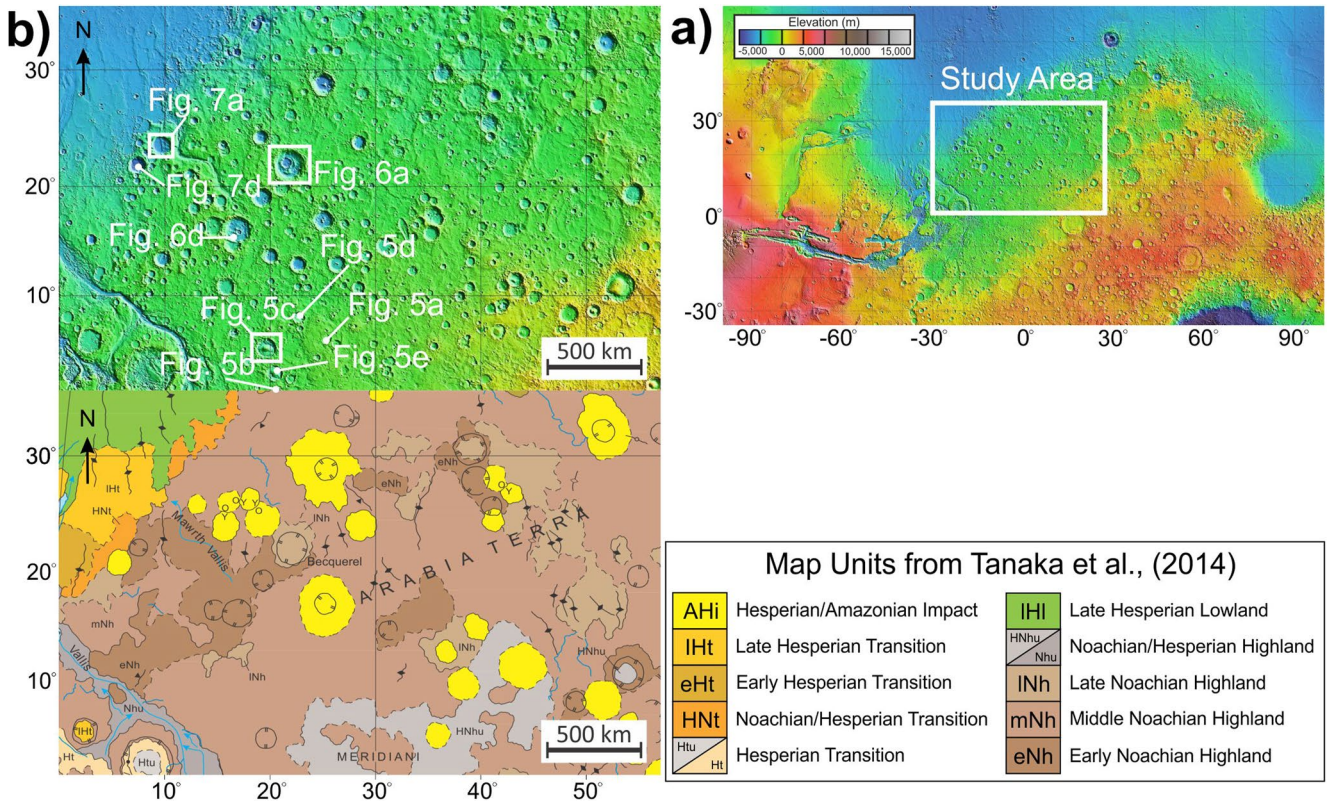

Figure 1. (a) MOLA-colorized DEM showing the location of the study area. (b) Close-up of the study area marked by the white square in Figure 1a with the corresponding section of Tanaka et al., (2014) global geological map of Mars. Locations of Figures 5–7 are marked.

activity (Andrews-Hanna et al., 2007, 2010; Bishop et al., 2008; Day et al., 2016; Evans et al., 2010; Lewis & Aharonson et al., 2014; Molina et al., 2017; Pondrelli et al., 2015; Salese et al., 2019; Silvestro et al., 2021; Whelley et al., 2021). These processes have produced a plethora of features including meandering valleys and deltas (Bishop et al., 2008; Molina et al., 2017; Salese et al., 2019). Additionally, many have proposed the existence of an ocean in the northern hemisphere and interpreted the western side of AT to represent a shoreline (Di Achille & Hynek, 2010; Rodriguez et al., 2016; Webb, 2004). The landing site of the ESA/ROSCOSMOS ExoMars 2022 rover was ultimately selected in Oxia Planum (Vago et al., 2015, 2017), an area of western Arabia Terra, based on the rich assembledge of fluvial geomorphology, sedimentary deposits, and hydrated mineral detections (Lakdawalla, 2019; Quantin-Nataf et al., 2021).

AT and its surroundings have a nearly two decade long history of aqueous mineral detection. Approximately 250 km south of the mapping area, in Meridiani Planum, sulfur-rich sedimentary deposits and layered sandstones were studied in-situ by the Opportunity Rover in Eagle crater, and phyllosilicates in the rim of Endeavour crater. Datasets from the Visible and Infrared Mineralogical Mapping Spectrometer (OMEGA) likewise revealed sulfates (Arvidson et al., 2005; Gendrin et al., 2005; Griffes et al., 2007; Poulet et al., 2008) and phyllosilicates (Noe Dobrea et al., 2012; Poulet et al., 2008; Wray et al., 2011; Wiseman et al., 2010). In the northwest area of the mapping area of Oxia Planum, detections in the valley network Mawrth Vallis demonstrated the abundance of sulfates from the Compact Reconnaissance Imaging Spectrometer for Mars (CRISM) (Noe Dobrea et al., 2011) and phyllosilicates from both OMEGA (Loizeau et al., 2010) and CRISM (Bishop et al., 2008; Loizeau et al., 2012, 2015; Wray et al., 2008), as well as a mixture of assemblages which represented changing environments (Bishop et al., 2020). Additionally, phyllosilicates have been detected within nearby Mclaughlin crater (Gou et al., 2014; Michalski et al., 2013, 2019) and even serpentine (Michalski et al., 2019). This rich assemblage ultimately led to the selection of Oxia Planum for the ExoMars rover landing site, which will continue with in-situ spectral analyses of layered deposits. Unfortunately, AT tends to have a layer of dust that covers the interior of the craters and their ELDs, impeding the extraction of reliable spectra in the other four observations (Mangold et al., 2009). Thus, the reliability of CRISM

datasets is severely inhibited in the study area. However, regardless of this dust hindrance, the association of ELDs with aqueous minerals is certain and their implications to past climate and water on Mars is well established.

The possible importance of groundwater either in directly contributing to the ELD deposition or in favoring their preservation through cementation has been proposed by Andrews-Hanna et al. (2007, 2010), Franchi et al. (2014, 2020), Michalski et al. (2013), Newsom et al. (2003), Oehler and Allen (2010), Pondrelli et al. (2011, 2015, 2019), Pozzobon et al. (2019), Rossi et al. (2008), Salese et al. (2019), and Zabrusky et al. (2012). The topographic characteristics of the region (i.e., absence of a dichotomic boundary, but gradual and gentle decreasing in elevation from the Southern Highland to the Northern Lowlands) make AT the best geological setting to investigate the potential relation between groundwater presence/fluctuations and ELD deposition/preservation. For these reasons, AT was chosen as the study area since the dozens of ELDs residing here across such a wide area (>2,000,000 km^2) provides a great opportunity to observe region wide trends which might yield important clues to the history of water on Mars.

We aim at providing regional constraints on the controls and processes leading to ELD deposition by identifying the distribution (latitude/longitude and elevation) of the ELD deposits within the craters in AT, the geometrical patterns within the different basins (e.g., thickness and height of the stratigraphic boundaries), and the association with main morphological elements (e.g., channel, mounds). The goal is to understand in detail the depositional and aqueous history of Mars. We also investigate the layer thicknesses variations in order to recognize possible common trends. Here the goal is understanding whether the controls on deposition and/or preservation are in common or localized, while alluding to the location of the source area of the sediments. Layer thicknesses of ELDs within single craters such as Bequerel, Crommelin, Danielson, Sera, and Jiji (Annex & Lewis et al., 2020; Cadieux & Kah, 2015; Lewis & Aharonson, 2014), as well as Kotido crater (Pondrelli et al., 2019), have been measured previously. These are reexamined and holistically considered in this study with the addition of new measurements from other ELDs, extending the scope and understanding of the stratigraphic section across the entire AT in order to better constraint their genesis and climate implications in the Martian evolutionary history.

3. Materials and Methods

3.1. Data

A Context Camera (CTX; 6 m/pixel) (Malin et al., 2007a) mosaic registered to a High-Resolution Stereo Camera (HRSC; 50 m/pixel) (Jaumann et al., 2007; Neukum & Jaumann, 2004) composite digital elevation model (DEM) of the eastern side of the MC-11 quadrangle (U.S. Geological Survey, 1973) forms the base data for the study. A Mars Orbiter Laser Altimeter (MOLA; 463 m/pixel) (Smith et al., 1999) DEM was used for observing topography of MC-12 (Coles et al., 2019), but was not used for direct measurements. Large scale measurements including crater depths and total deposit thicknesses were obtained using HRSC elevation data. These measurements were then compared to the results obtained from the Garvin equations (Garvin et al., 2003). Small-scale landforms and layering were examined within High-Resolution Imaging Science Experiment (HiRISE) stereo imagery (100–40 cm/pixel) (McEwen et al., 2007). All layer attitude and thickness measurements were obtained from HiRISE DEMs computed in house using the NASA AMES Stereo Pipeline (Shean et al., 2016).

3.2. Garvin Equations

Deposit thicknesses were determined by the elevation difference between the highest and lowest areas of the deposit. Crater depth was determined by the elevation difference between the crater rim and the lowest area of the crater floor. Each measured crater depth was then compared to those determined by the Garvin equations which are a set of crater diameter (D) versus crater depth (d) power laws (Garvin et al., 2000; 2003):

$$d = 0.36 \cdot D^{0.4} (7 < D < 100\ \text{km})$$

$$d = 1.27 \cdot D^{0.21} (D < 100\ \text{km})$$

By comparing the measured crater depth values to those determined by the Garvin equations, it can be inferred which craters might be deeper than is measurable due to deposit infill covering the true crater floor. This difference can then be used as a reference for certain deposits that might have significant sections buried, which implies the deposit is thicker than what can be measured.

3.3. Measuring Layer Thicknesses

Several studies have previously described the fundamentals of obtaining layer thickness and attitude from orbital data in an effort to find stratigraphic trends within layered deposits across Mars (e.g., Fueten et al., 2014, 2008; Lewis & Aharonson, 2014; Lewis et al., 2008). In 19 HiRISE stereo pairs covering 13 craters containing ELDs, layer thicknesses were obtained by measuring elevation and distance between each layer along a line parallel to slope within the GIS software Global Mapper (Blue Marble Geographics, 2011). The resulting measurements had an average error of ±0.4 m, a combination of vertical resolution and the placement of points on layer edges (in general, error decreases with thickness). Multiple transects were measured within each HiRISE image. A total of 1,237 layer thickness measurements were taken along 231 transects.

Accurate layer thickness measurements are obtained by correcting for the dip of the layers. Depending on dip direction, dips will result in measured layer thicknesses either higher or lower than the true layer thickness. Horizontal distance between two points can affect the measured layer thicknesses greatly. Large horizontal distances create larger errors, even if the dip is shallow. To correct for dip and minimize error, the tangent of the dip angle is multiplied by the horizontal distance x between two points and then subtracted from their vertical distance y. This value is then multiplied by the cosine of the dip angle:

$$\left(y - \left(\tan\left(\phi\right) \cdot x\right)\right) \cdot \cos\left(\phi\right)$$

Dips were obtained using the Orion software (Pangaea Scientific, 2011). AT has extensive dust cover which can obscure thinner layers and create the illusion of thicker layering which in reality are benches able to project through the veneer of dust. Thus, all layers are selected manually by observing elevation relief and their horizontal continuation. Transects are chosen by identifying the path of least obstruction. No transects passed through fold hinges where significant error can occur from changing lateral thickness. Layers are not selected based on alternating albedo or a computer algorithm (Table 1).

Jiji North contains layering associated with the ejecta blanket of a secondary crater in the center of the crater. These layers were measured as well and included although we recognize their origin may be wholly separate from ELDs in other craters. Jiji North does contain ELDs in the southeast area of the floor adjacent from to the crater wall, but is not covered by HiRISE. The layers were measured with CTX elevation data and presented in the supplementary data.

4. Results

4.1. Crater Categorization and Deposit Distribution

A total of 1,013 craters were examined in the mapping area and categorized into six types according to morphologic features and the characteristics of any present infilling (Figures 2 and 3a). Crater types were not based on size or age, thus each of the six types can have a wide range of crater ages (Mangold, Adeli, et al., 2012) All craters resolvable in CTX imagery and with diameters >1.5 km were considered. These six types of craters are: ELD bearing, flat-floor, impact deposits, central peak, featureless, and uncertain. ELDs were observed in 79, a flat-floor (craters with a flat-topped infilling) in 43, impact deposits in 34 (craters filled at least partially with impact ejecta), a central peak (non-depositional related to the impact process) in 252, 548 featureless craters (Figures 2 and 3). The uncertain crater type describes 60 craters that had a degree of uncertainty (generally due to lack of high resolution imagery) of whether what was observed is an ELD, an impact deposit, or a central peak. Flat-floor craters have a distinctly high thermal inertia and are evenly filled (perhaps by lava) almost to the crater rim. Featureless craters vary from flat to bowl shaped topography, however those with flat topographies do not have the high thermal inertia indicative of the flat-floor crater type. Measurements were focused on 45 ELD craters in the MC-11 quadrangle and were categorized into three groups characterized by their geographic location and grouping. The three groups,

Table 1
HiRISE Stereo Pairs Used to Measure Layer Thicknesses Displayed in Figure 9. The Crater Names That Each of the Stereo Pairs Cover is Indicated, as Well as the Total Number of Transects and Individual Layer Measurements

Stereo pair	Crater	No. of transects	No. of measurements
ESP_042991_2020 ESP_043136_2020	McLaughlin	5	23
ESP_040222_2020 ESP_040367_2020	McLaughlin	2	13
ESP_040156_2020 ESP_040512_2020	McLaughlin	5	15
ESP_033391_2020 ESP_037149_2020	McLaughlin	2	8
ESP_028354_2025 ESP_043070_2025	McLaughlin	4	17
PSP_007599_2020 PSP_007454_2020	McLaughlin	5	17
ESP_022288_2035 ESP_022354_2035	Oyama	12	83
ESP_020811_1955 ESP_020956_1955	Trouvelot	13	50
PSP_001546_2015 PSP_001955_2015	Becquerel	15	173
PSP_001546_2015 PSP_001955_2015	Becquerel B	10	98
PSP_003788_1820 ESP_020679_1820	Firsoff	8	30
PSP_008416_1830 PSP_008772_1830	Firsoff	19	58
ESP_016776_1810 ESP_016921_1810	Kotido	3	13
PSP_002733_1880 PSP_002878_1880	Danielson	13	109
PSP_002047_1890 PSP_001902_1890	Sera	24	122
ESP_037267_1890 ESP_037834_1890	Sera	13	59
ESP_057245_1890 ESP_057456_1890	Sera	14	72
ESP_017013_1880 ESP_016657_1890	Jiji South	50	215
ESP_019347_1890 ESP_037267_1890	Jiji North	9	25
B18_016657_1881 B19_017013_1881	Jiji North	5	37

named Lower Mawrth, Upper Mawrth, and Southern Region, are relatively isolated from each other and reside at differing elevations of −5,100 to −3,900 m, −4,400 to −3,000 m, and −3,300 to −1,900 m respectively.

Layered deposits of Meridiani Planum were not considered for this study in order to better constrain those of AT, although this study recognizes the likelihood of a shared origin between them. The exact boundary between AT and Meridiani Planum is not well defined and therefore several ELDs at or within 100 km of the marked boundary in Figure 3 were also measured.

4.2. Layered Deposit Groups

We grouped the 45 craters containing ELDs within the area outlined by the white-dashed line in Figure 3a into three groups: Southern Region, Upper Mawrth, and Lower Mawrth (Figure 4). ELDs were placed into these three groups based on their location and the similarities shared between deposits within each group. The total thickness of ELDs within craters from the three groups decreases from the southeast to the northwest. Southern Region craters have the highest average deposit thickness of 485 m. Upper Mawrth craters have an average deposit thickness of 333 m. Lower Mawrth craters have the lowest average deposit thickness of 160 m (Table 2). Furthermore, there are a variety of morphological and structural differences between the three groups.

The Southern Region deposits (e.g., Figure 5) are not only very thick (observable thickness avg. = 456 m), but also cover a large percentage of the crater floor, in some cases entirely (e.g., Kotido and Crommelin). In some instances, there are prominent central mounds (e.g., Crommelin and Firsoff), while in others the deposit favors one side (e.g., Sera, Jiji North, Jiji South, and Vernal) or even two sides as seen in Danielson. The deposits often are eroded into buttes (e.g., Sera and Jiji South) and bedding exhibits layers of high and low resistance to erosion creating saw tooth patterns. Deposits often have small conical mounds superimposed

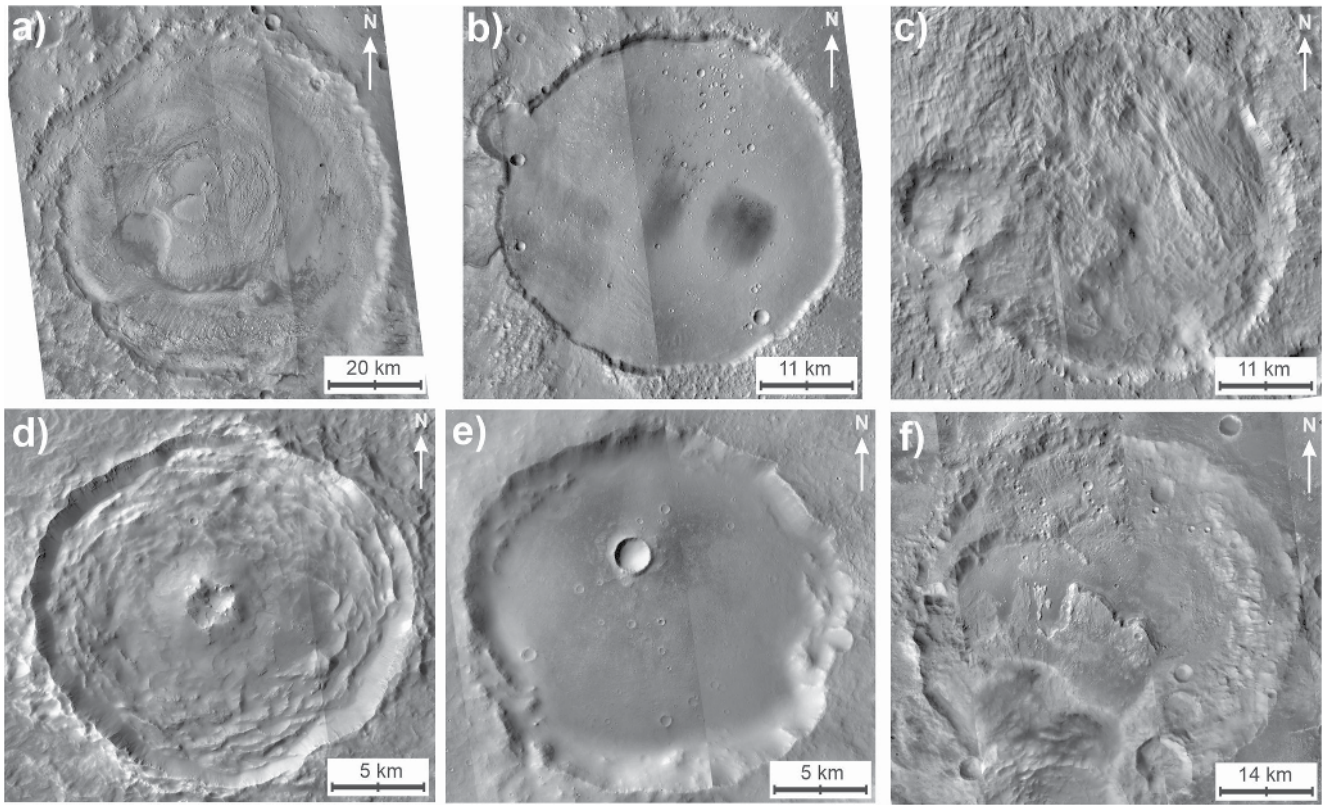

Figure 2. Examples of the six crater types featured in the crater identification map of Figure 3. All examples are presented in CTX imagery. (a) Equatorial layered deposit (ELD) (2.6°, −9.3°). (b) Flat-floor (3.5°, −14.2°). (c) Impact deposit (7.1°, 21.3°). (d) Central peak (21.5°, −1.5°). (e) Featureless. (f) Uncertain (18.7°, −15.6°).

(Franchi et al., 2014; Pondrelli et al., 2011, 2015, 2019; Pozzobon et al., 2019) (Figure 5b). Deposits show varying thinning and thickening bedding sequences, faulting, folding, layer dips >30° (Figure 5d).

Upper Mawrth craters (e.g., Figure 6) show intermediate characters between the other groups not only in terms of average thickness (observable thickness avg. 302 m). They do not cover the entire crater floor but show locally extensive ELD sequences. Within Becquerel and Trouvelot ELD form mounds that are obliquely shaped and emplaced off center from the crater, each in the southeastern side of the crater. Upper Mawrth deposits appear to have been more susceptible to aeolian erosion than the other groups as is evidenced by a higher occurrence of yardangs, particularly within Trovoulet (linear features that trend SW-NE in Figure 6a).

Deposits within the Lower Mawrth craters (e.g., Figure 7) are thinner (observable thickness avg. = 160 m) and generally have a patchy appearance with no predictable distribution. They appear more friable and brittle in respect to the other groups. However, there are instances where layered buttes have formed (Figure 7b). Also, albedo contrast between layering is more extreme than the other groups (e.g., Figure 7c).

The difference between the inferred depth (derived from Garvin equations) and the measured depth (Table 2) can be a simple way to view the hypothetical thickness of a deposit in cases where the lower sections of the deposit are not observable due to burial. The resulting inferred deposit thicknesses have averages of 789 m (Southern Region), 174 m (Upper Mawrth), and 513 m (Lower Mawrth). However, these values do not accurately describe every situation, notably Trouvelot and Rutherford (both in the Upper Mawrth crater group) where observable depth was greater than the inferred depth. Therefore the observed deposit thicknesses are taken at face value, while considering the importance of the inferred deposit thicknesses in individual circumstances.

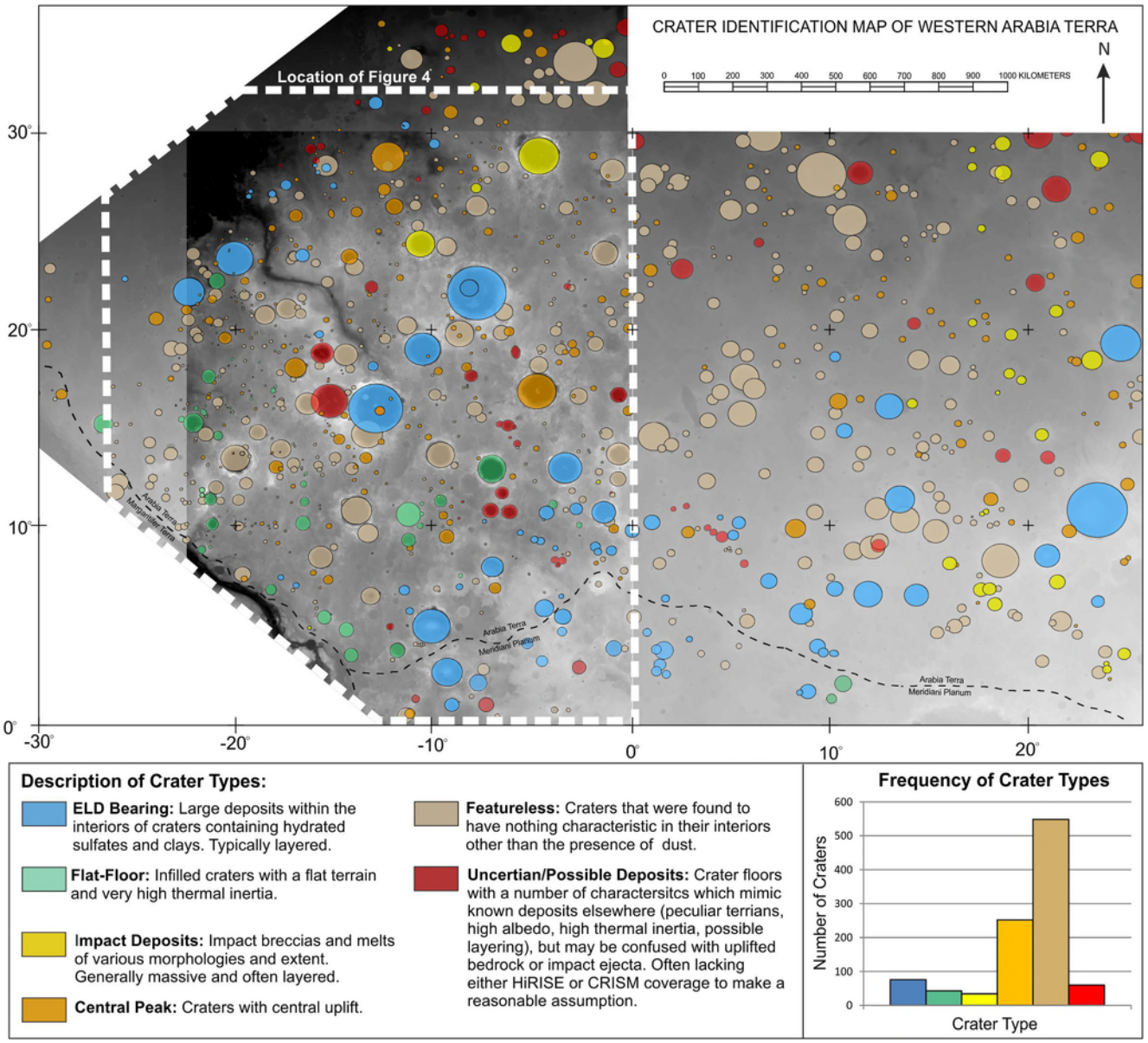

Figure 3. A crater identification map of the six crater types showing their distribution and frequency. Color-coded crater identifications are shown over a grayscale HRSC and MOLA DEMs. The white-dashed box represents the location of Figure 4. A frequency graph shows the quantity of each crater type.

4.3. Measurements and Trends

Measurements reported in Table 2 were used to compare each deposit thickness to the diameter, depth, elevation, and latitude of the crater they are contained in. Measurements revealed positive correlations between deposit thickness and the crater depth, diameter and latitude (Figures 8a and 8b). These correlations are more apparent within the Southern Region and Upper Mawrth deposits, whereas the Lower Mawrth deposits maintained lower thicknesses regardless of crater size. Elevation of the crater rim and floor do not appear to be major influences on the thickness of the deposit (Figures 8c and 8d). Deposits tend to not be associated with a central peak (formed from impact) nor do they tend to form centered layered mounds; rather deposits are more often in either an irregular spatial position within the crater (e.g., Becquerel, Trouvelot, Jiji) or cover the crater floor evenly (e.g., Kotido). Uniquely, Rutherford and Trouvelot are observed 612–743 m deeper than their inferred depths produced by the Garvin equations. All other craters have observable depths either equivalent or, more commonly, shallower than the inferred depths.

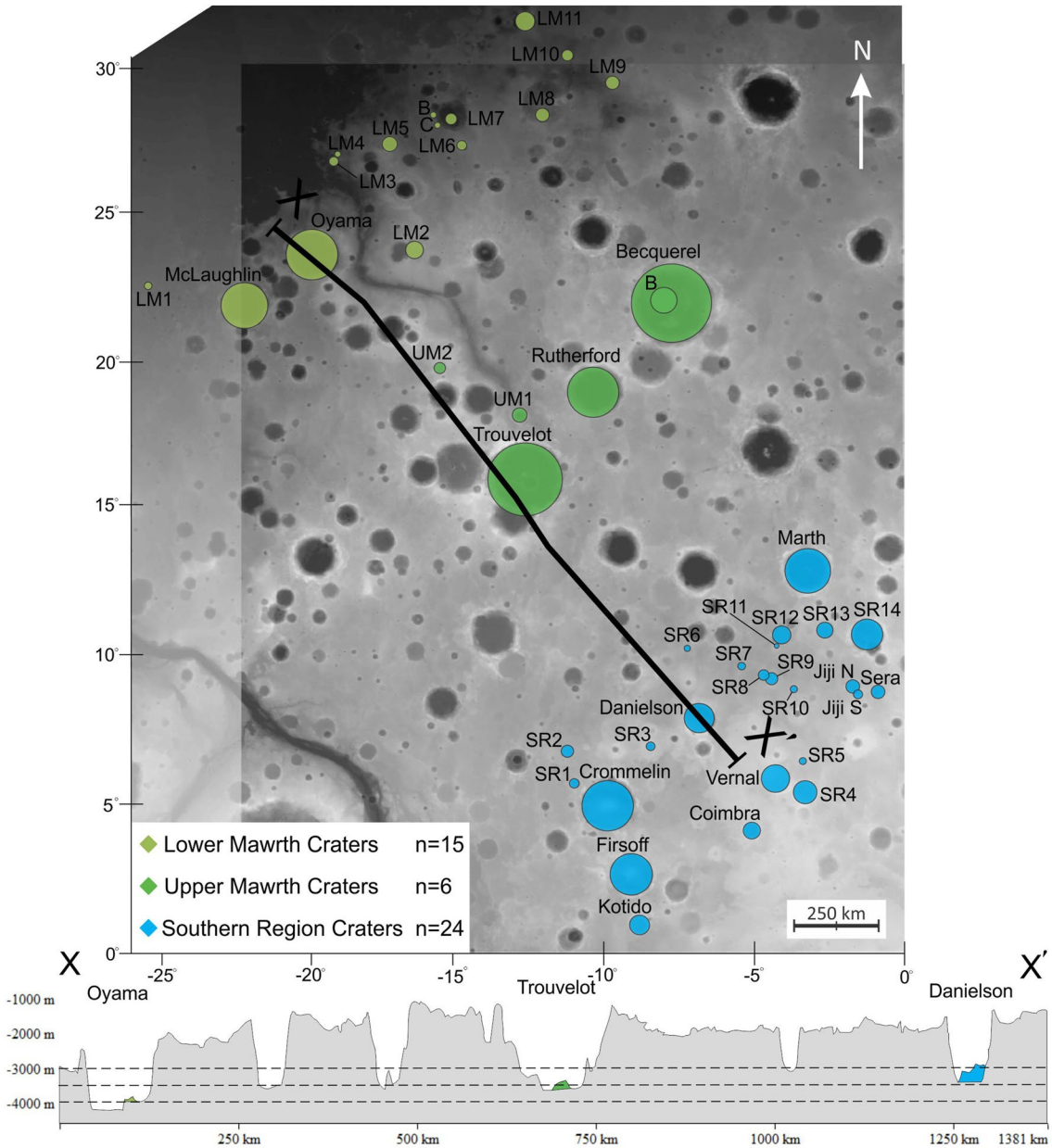

Figure 4. 45 craters containing equatorial layered deposits (ELDs) within the MC-11 quadrangle are classified into three groups: Southern Region (blue), Upper Mawrth (dark green), and Lower Mawrth (light green). Background: Grayscale HRSC DEM and MOLA DEM mosaics. Cross-section X-X', located approximately parallel to the regional slope of the land, shows the broad elevation change in crater depth across the study area and the relative difference of deposit thickness between the three groups.

Of the 45 ELD craters measured from the MC-11 quadrangle (Figures 4 and 8 and Table 2), 13 were measured with 19 available HiRISE stereo pairs to determine layer thicknesses. The distribution of the layer thickness measurements is shown in Figure 9. A total of 1,237 layer thicknesses were measured, and although the number of measurements taken from each group is not equal due to the distribution of available HiRISE stereo pairs, we suggest that southeast-northwest trends are present.

Similar to deposit thicknesses, layer thicknesses decrease from the southeast to the northwest (Figure 9). Southern Region craters have the highest average layer thicknesses of 8.05 m and range 1.49–24.44 m. Upper Mawrth craters have average layer thicknesses of 5.12 m and range 3.76–14.63 m. Lower Mawrth craters have the lowest average layer thicknesses of 1.73 m and range 0.12–6.66 m. In general, the thicker deposits

Table 2
List of All Measured Dimensions of the 45 Craters That Were Put Into the Three Groups: Southern Region (blue), Upper Mawrth (Dark Green), and Lower Mawrth (Light Green)

Crater	Location	Diameter (m)	Inferred Depth (m)	Observed Depth (m)	Rim Elevation (m)	Observed Floor Elevation (m)	Uppermost Elevation of the ELD (m)	Observed Deposit Thickness (m)
Coimbra	4.1, -5.3	34205	2032	1819	-806	-2625	-2212	413
Crommel	4.9, -10.1	109895	2232	2206	-1341	-3547	-1402	2145
Danielson	8.0, -7.0	59870	2674	1975	-1500	-3475	-1900	1575
Firsoff	2.7, -9.4	84050	3157	1839	-1361	-3200	-1484	1716
Jiji North	9.1, -1.9	28975	1874	966	-1535	-2501	-2370	131
Jiji South	8.8, -1.7	21536	1620	1041	-1500	-2541	-1875	666
Kotido	1.0, -9.11	40939	2219	1094	-1500	-2594	-2349	245
Marth	12.9, -3.4	98622	3415	2272	-1134	-3406	-3281	125
Sera	8.83, -1.0	30263	1914	1054	-1539	-2593	-1905	688
Vernal	5.9, -4.4	54315	2549	979	-1005	-1984	-1755	229
SR1	5.7, -11.2	20639	1587	1299	-1524	-2823	-2550	273
SR2	6.8, -11,5	29700	1897	676	-1840	-2516	-2150	300
SR3	7.0, -8.7	20003	1563	1602	-1349	-2951	-2500	100
SR4	5.4,-3.5	47059	2376	1138	-1111	-2249	-2037	212
SR5	6.5, -3.6	15216	1367	955	-1147	-2102	-2027	65
SR6	10.3, -7.5	11148	1173	568	-1901	-2469	-2266	203
SR7	9.7, -5.6	17306	1456	901	-1795	-2696	-2436	260
SR8	9.4, -4.9	23797	1701	769	-1875	-2644	-2280	205
SR9	9.3, -4.6	23671	1697	726	-1750	-2476	-2092	384
SR10	8.9, -3.9	15372	1373	471	-1750	-2221	-1943	278
SR11	10.4, -4.5	8066	1001	668	-1638	-2306	-2280	26
SR12	10.7, -4.3	40568	2210	1064	-1750	-2814	-2592	222
SR13	10.9, -2.8	33786	2020	1125	-1530	-2655	-2211	444
SR14	10.8, -1.5	70582	2898	1863	-1301	-3164	-3094	30
Group Average		39149	2000	1211	-1478	-2690	-2208	456
Becquere	21.3, -8.1	162520	2339	2341	-1500	-3841	-2856	800
Becquere	21.9, -8.2	53002	2519	1021	-3250	-4271	-4118	153
Rutherfor	8.8, -10.5	110070	2233	2845	-1250	-4095	-3625	470
Trouvelot	6.1, -13.0	135993	2290	3033	-1000	-4033	-3386	267
UM1	8.1, -13.1	26627	1798	1602	-1800	-3402	-3350	28
UM2	9.7, -15.8	20530	1583	873	-1462	-2335	-2242	93
Group Average		84790	2127	1953	-1710	-3663	-3263	302
McLaughl	1.9, -22.4	88731	3242	2555	-2500	-5055	-4887	168
Oyama	3.5, -20.1	102570	2214	1932	-2250	-4182	-3805	150

Note. Inferred Depth is calculated using the Garvin power law equations described in Section 3.2. The difference between the Inferred Depth and the Observed Depth can be used to suggest the thickness of an equatorial layered deposit (ELD). The craters can be located by their coordinates and by referencing Figure 4.

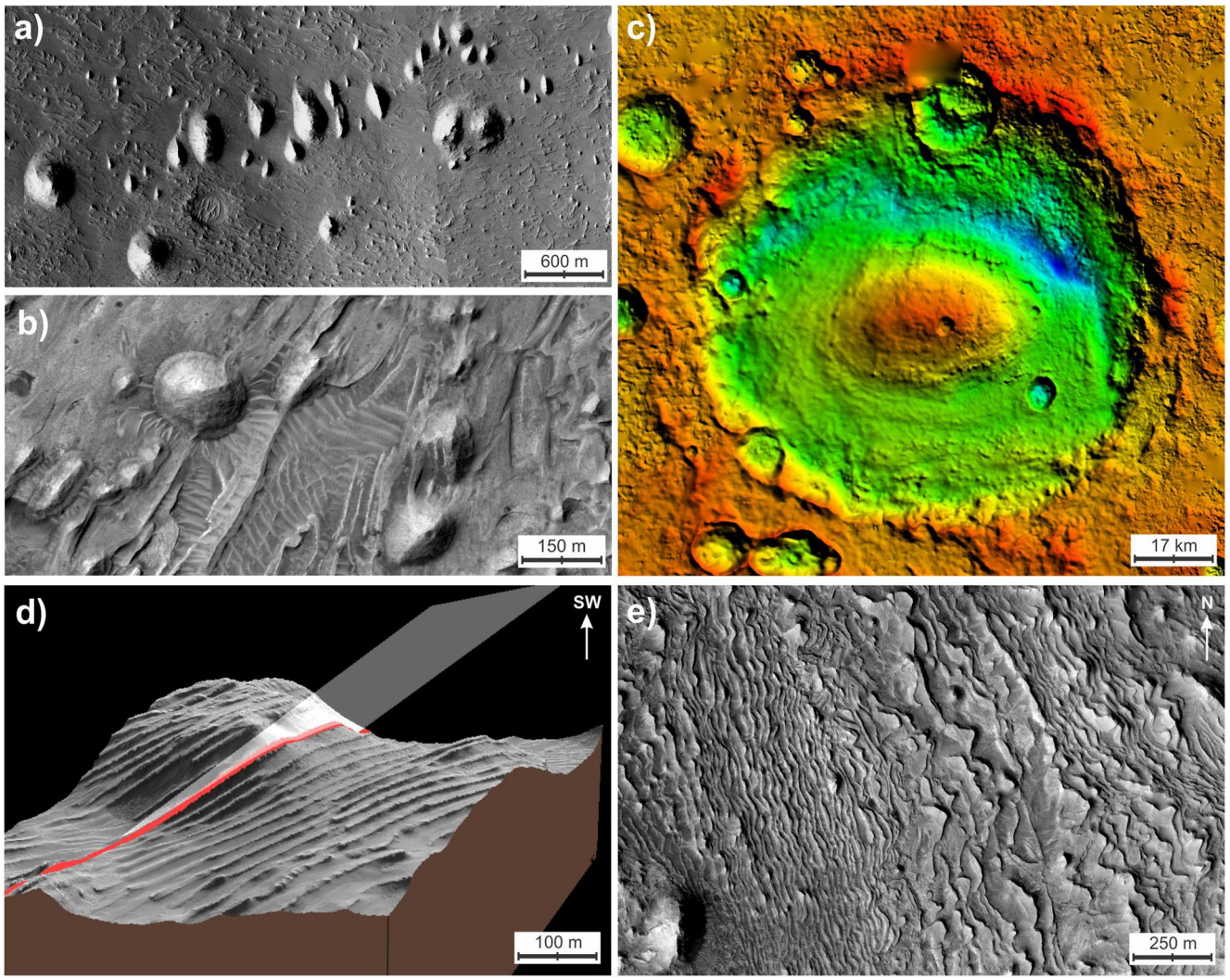

Figure 5. Example imagery of the Southern Region deposits. (a) Group of smaller mounds (some show layering) superimposed upon a larger equatorial layered deposit (ELD) within Vernal. (b) Example of layerless mounds superimposed upon a larger ELD within Kotido. (c) HRSC topography of Crommelin showing the massive ELD mound which fills the crater and reaches the rim in height. (d) 3D view of the high layer attitudes that can be present in some craters, in the case Danielson. The red line represents the trace of a layer. The transparent plane which extends outward represents the bedding plane associated with the layer. (e) Example of laterally continuous layering within Firsoff.

tended to have thicker layering (Figure 8f). Various thinning and thickening sequences were observed regionally and within individual deposits. Regionally, thickening from −4,000 to −3,500 m, thinning from −3,500 to −3,300 m, thickening from −3,000 to −2,400 m, and thinning from −2,400 to −2,000 m was observed (Figure 9a). Furthermore, the putative long-term water level of −4,000 m (Salese et al., 2019) correlates well with a change of average layer thickness from 5.11 m (average of layer thickness at elevations from −3600 to −3300 m) to 1.60 m (average layer thickness at elevation from −4,100 to −5,100) (Figure 9a).

Our layer thickness measurement averages match well with those done previously in some of these craters (e.g., Annex & Lewis, 2020; Cadieux & Kah, 2015; Lewis & Aharonson, 2014, 2008). Measurements also reveal that the range of thicknesses and amount of thinning and thickening sequences within these deposits is more complicated than the measurements presented in Annex and Lewis (2020), which is a reflection of our measurements covering more craters to the northwest and at lower elevations. Our measurements in Kotido and those presented in Pondrelli et al. (2019) seem to match the unit described in Annex and Lewis (2020) present within the craters Kaporo, Yelapa, Wulai, and Alofi further west of our study.

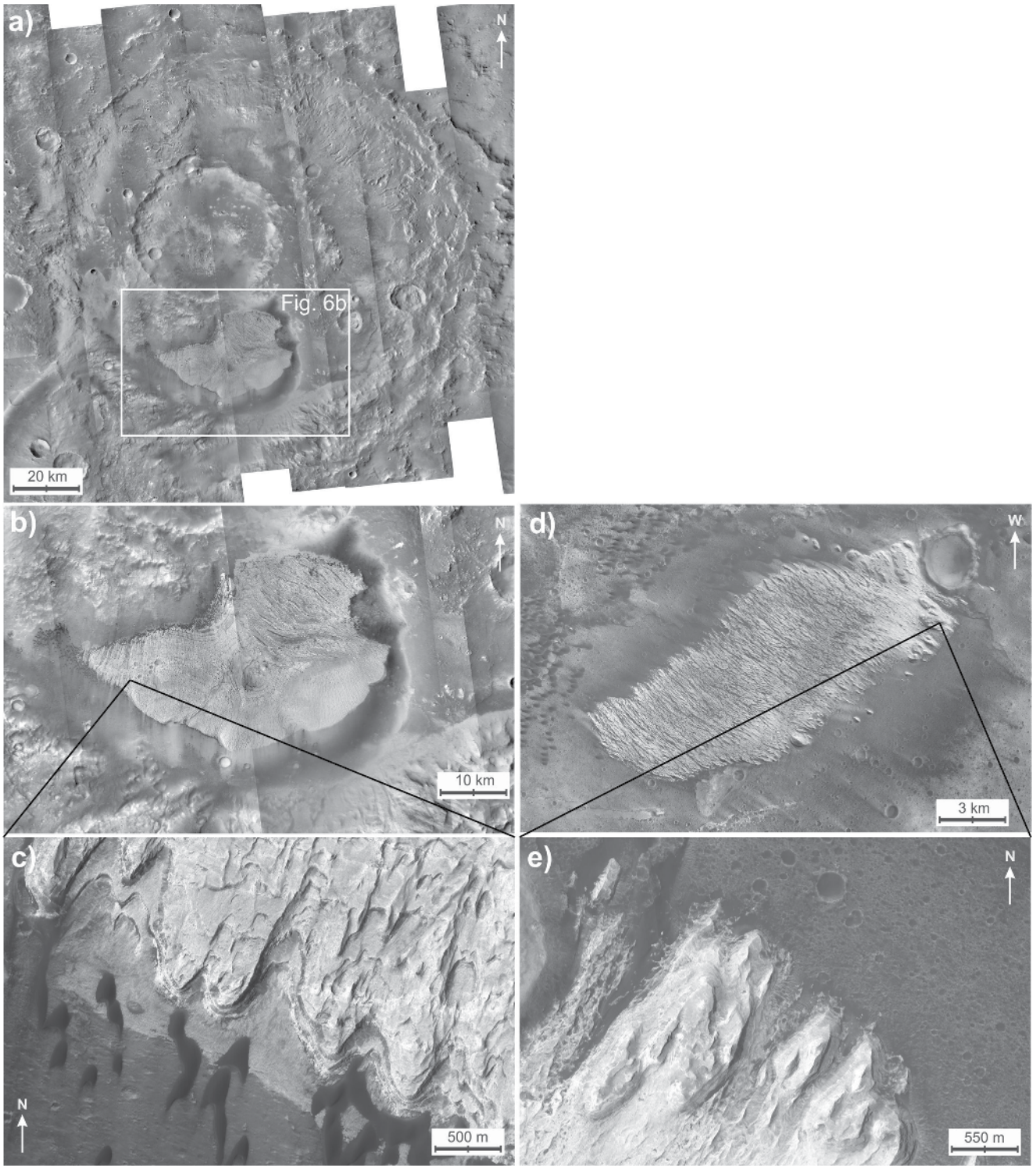

Figure 6. Example imagery of the Upper Mawrth deposits. (a) Becquerel crater and the secondary crater "Becquerel B". White box locates the high albedo isolated ELD mound. (b) The high albedo, isolated ELD mound within Becquerel. (c) Close-up of figure (b. (d) The high albedo, isolated ELD mound of Trouvelot. Yardangs trend SW-NE across the ELD mound surface. (e) Close-up of figure (d).

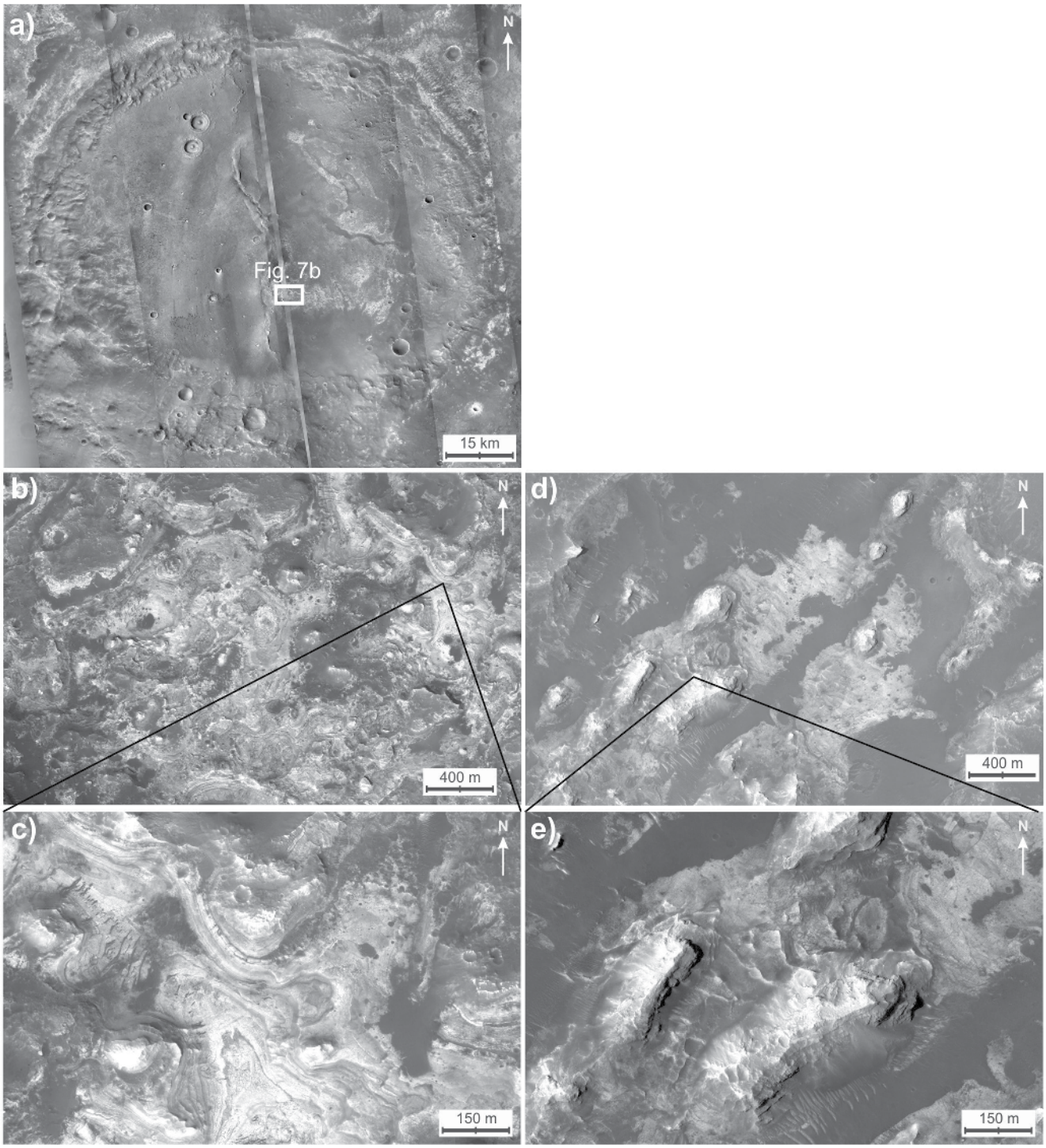

Figure 7. Example imagery of the Lower Mawrth deposits. (A) Oyama crater. (b) Layering within Oyama. (b) Close up of figure (b). (d) Layered buttes within McLaughlin. (e) Close up of figure (d).

Jiji North contains two separate ELDs, one associated with the rim of a secondary crater (thickness = 131 m, layer thickness avg. = 8.32) and another separate ELD observed on the south-southwest side (thickness = 250 m, layer thickness avg. = 9.56). The association with a secondary crater and small thickness (131 m) is evidence that it is a pedestal crater deposit. The other ELD lacks HiRISE coverage, but was

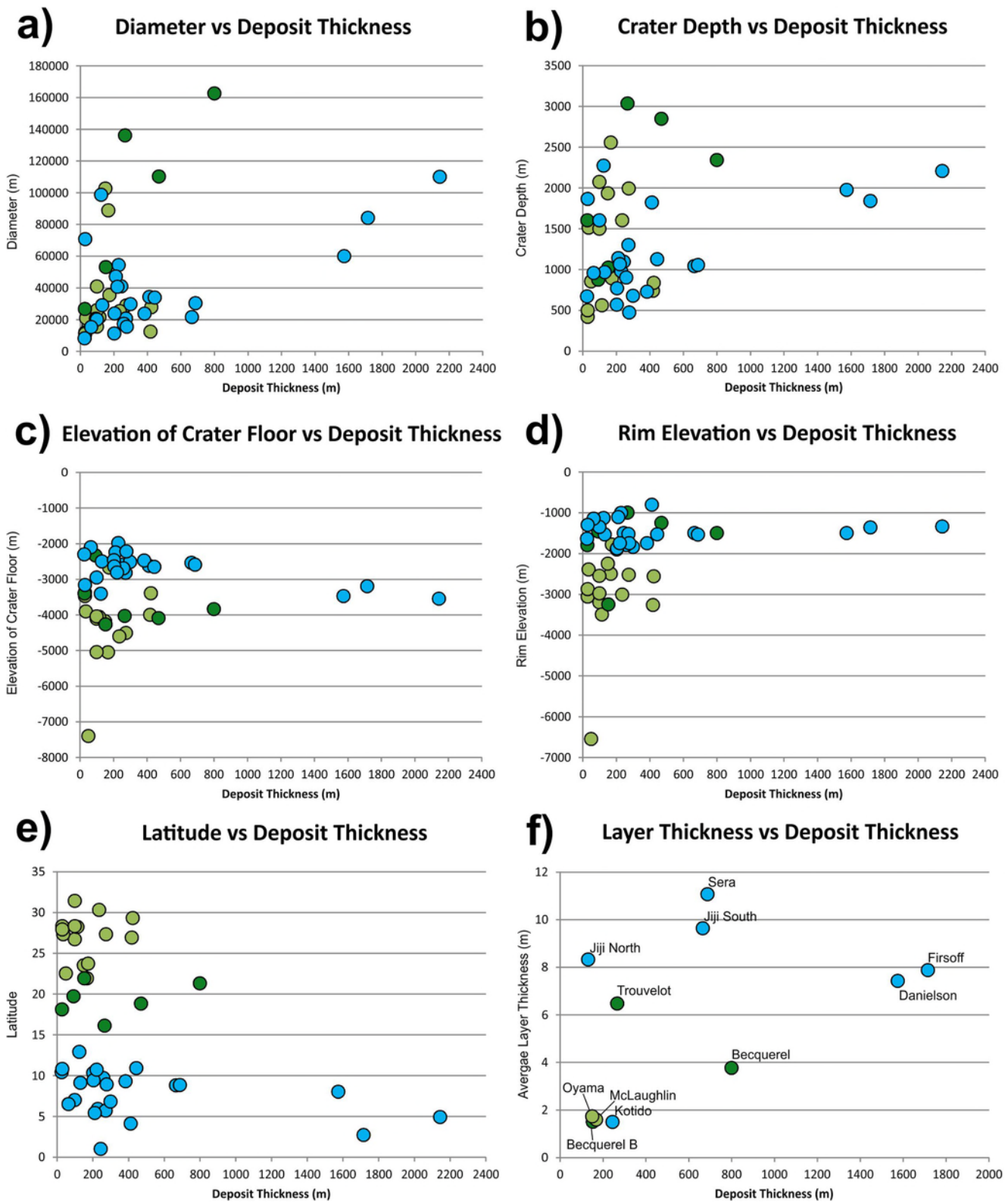

Figure 8. Deposit thickness graphs using measurements from the "Observed Deposit Thickness" column in Table 2. Figure 8f uses layer thickness averages presented in Figure 9.

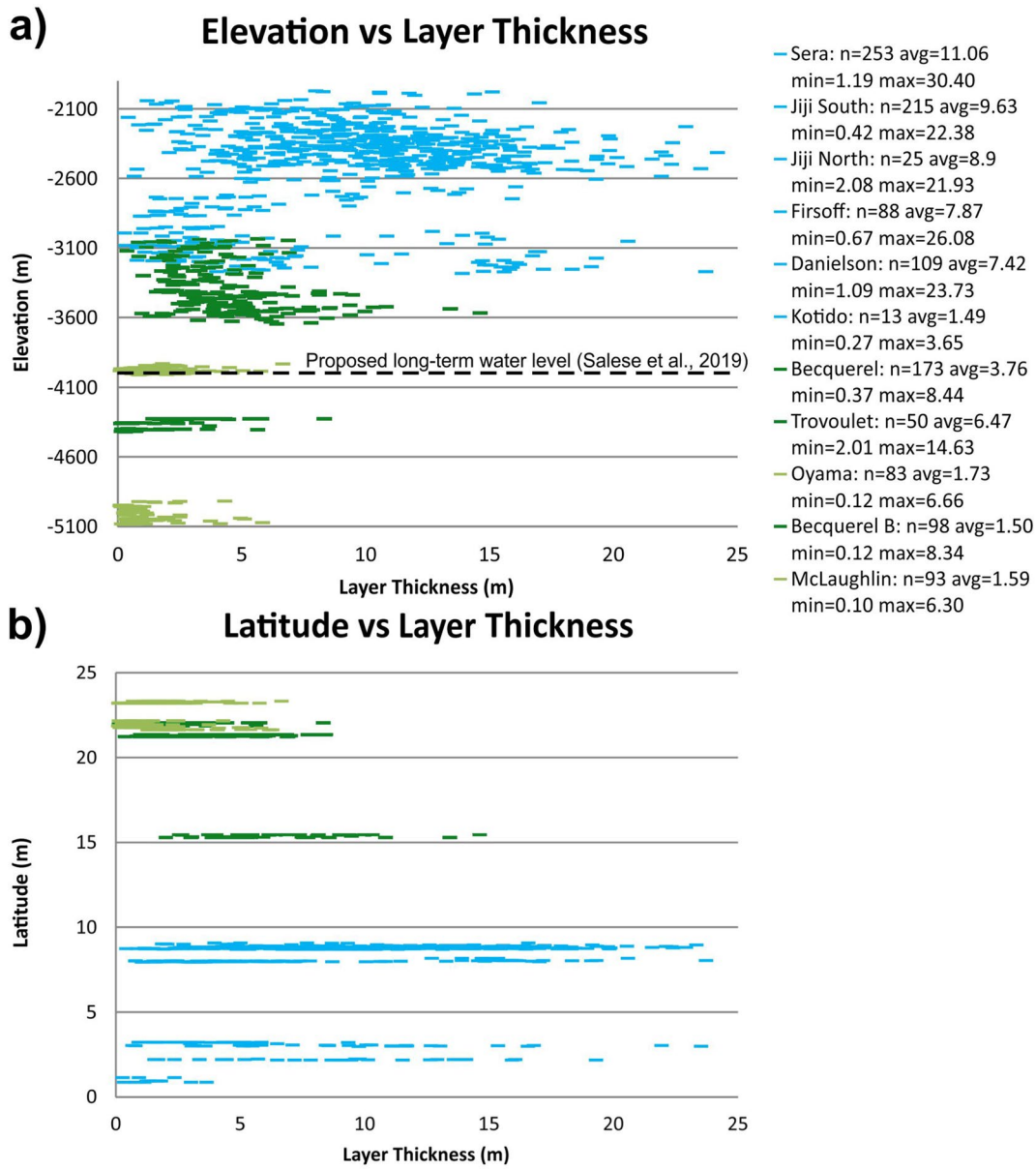

Figure 9. Graphs showing layer thickness. The legend corresponds to both graphs. Colors represent the three groups presented in Figure 4. Each measurement is placed as a horizontal dash to convey the ±0.4 m average error. (a) Elevation versus layer thickness graph with black dashed line marking the putative long-term water level presented in Salese et al. (2019). (b) Latitude versus layer thickness graph.

measured with CTX derived topography (supp. mat.) and matches well with those measured in Jiji South and Sera.

4.4. Layer Attitude Measurements

The layer attitudes vary across the region, but are generally sub-horizontal. As was observed in layer thicknesses, average dip values decrease southwest to northeast (Figure 10a). Although the majority of layers are sub-horizontal, there are many instances where layering exceeds dips of 10° and several unique craters with dips as high as 44° (e.g., Danielson, Firsoff, Sera, Becquerel, and Becquerel B) (Figure 10a). Layer dips of the Southern Region deposits range 0°–43° with an average of 6.9°. Layer dips of the Upper Mawrth deposits range 0°–44° with an average of 7.6°. Layer dips of the Lower Mawrth deposits range 0°–17° with an

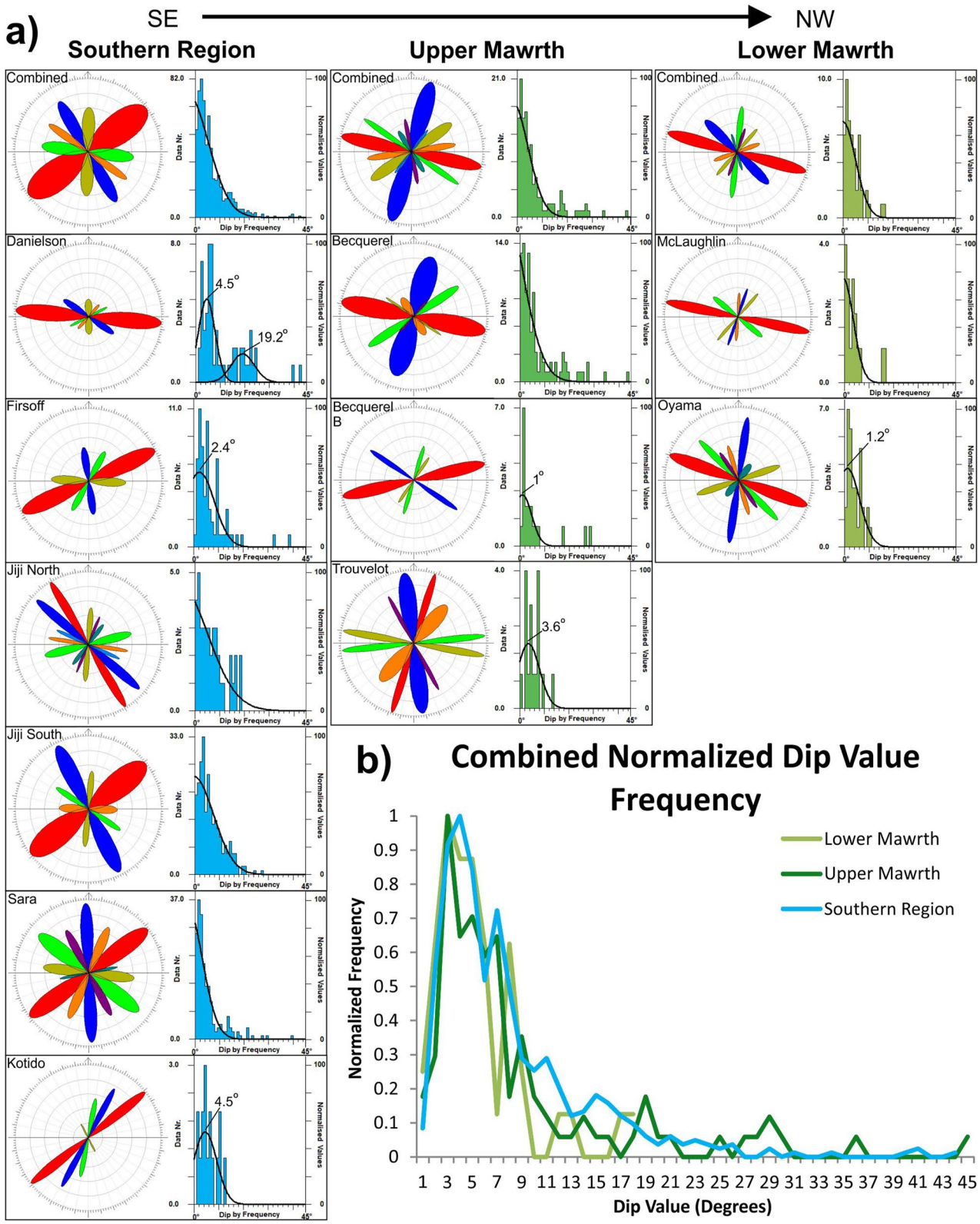

Figure 10. Layer attitude analysis. (a) Rose diagrams display preferred strike directions, color coded for distinguishability. Bar graphs display dip frequency with a superimposed black line showing the Gaussian curve of the data. Each column represents the three crater groups Southern Region, Upper Mawrth, and Lower Mawrth. The top row shows the combined data of the three groups. (b) Graph of dip value frequency for each of the three groups (frequency is normalized).

average of 4.5°. Interestingly, the Southern Region ELDs have a gradual decline in frequency as dip values increase, whereas the Upper Mawrth ELDs have chaotic fluctuations in frequency as dip values increase (Figure 10b). Statistical analysis of the dips revealed that the ELD with Danielson contains two groups of dips (averaging at 4.5° and 19.2°), which does not exist in the other craters measured.

Only rarely does dip exceed values that can be considered above the angle of repose of these materials. On Earth, the angle of repose varies depending on grain size roughly between 34° (dry sands) and 45° (dry gravel) which has been shown to be similar on Mars, at least in dry sands (Atwood-Stone and McEwen, 2013). Regardless, high dips measured in the Southern Region deposits are found within the limbs of folds in Danielson [mentioned previously by Murana (2018)], Firsoff, Kotido, Jiji South, and Sera. High dips in Becquerel and Becquerel B are not observed in association with folding, but rather deformation features similar to faulting, landslides, and collapse.

The dip directions (presented as strike in the rose diagrams of Figure 10a) do not show a particular direction when combined for each group (top row of Figure 10a), indicative of the majority of layering being sub-horizontal. However, ELDs of individual craters (e.g., Danielson, Firsoff, and Kotido) do show an overwhelming preferred dip direction.

5. Discussion

ELD distribution in AT has important implications for determining a variety of unresolved questions regarding the history of Mars. Due to their widespread occurrence and unique character, unraveling their distribution and relationships provides a significant contribution to understanding the past climates on Mars. It is unclear if the ELDs are formed by a unified depositional method or if layering is produced by different processes based on location. Central to these questions is determining precisely what controls the thickness of a layer and why some craters have thin layers while others have thick layers.

5.1. Regional Trends

5.1.1. Layer Thicknesses

Our measurements demonstrate that ELDs display distinct changes in morphology (Figures 5–7), deposit thickness (Figure 8e), and layer thickness (Figure 9) from the northwest to the southeast of the mapping area. This trend is somewhat complicated by the influence by other controls associated with crater dimensions (Figure 8), as well as by the presence of so many featureless craters (Figure 3a). The southeast to northwest decrease of both the average ELD thickness (from 456 to 302 m–160 m) and the average layer thicknesses (from 8.05 to 5.12 m to 1.73 m) suggest the presence of a latitude-dependent control or proximal-distal relationship to the source, while the relationship between crater dimensions and deposit thickness suggests in turn a relation with the accommodation space. However, many craters are left empty and different spatial placements of the ELDs within the craters are observed. For example, there is a significant difference between the off center, isolated mound of Becquerel (Figure 6b), and the large central mound which reaches the crater rim within Firsoff. Other differences include the positioning of the ELD within Danielson which resides on the NE and SW crater walls to the ELDs of both Jiji and Sera which resides mostly on the SE wall. Such varying spatial positions are even more peculiar when compared to the ELD within Kotido which has a relatively flat and observably thin deposit which covers the entire floor.

Layer thickness shows a significant change at the 15° latitude, which might signify an extent of reach of depositional processes effecting lower latitude craters (e.g., atmospheric dust saturation culminating around the equator). Additionally, this change is observed at an elevation of −4,000 m, the same elevation as the putative long-term water level (Salese et al., 2019), which might also represent a regime change due to standing water. The relationship between deposit thickness and crater dimension is pronounced in the Southern Region deposits, where deposit thickness increased with crater depth and diameter. It is less pronounced in the Upper Mawrth deposits and non-existent in the Lower Mawrth deposits, which suggests a change in environment and factors which influenced the depositions between the Southern Region and Lower Mawrth.

Measurements show that the thickness of a deposit is more heavily influenced by crater depth and latitude than by the rim elevation and floor elevation. Although craters with the lowest rim elevations have the thickest ELDs, the majority of craters do not show a significant correlation between these parameters (Figure 8d). Furthermore, rim elevation might have been greatly reduced by erosion over time thus revealing more details of this relationship will require an analysis of erosional rates acting on these rims. In the case that rim elevation did influence the ability for material to be deposited within a crater, we assume that higher rims would impede this. Since the majority of ELD thicknesses do not show a relationship with rim elevation, this might indicate the ability for material to pile up inside a crater could be influenced by the environment inside the crater (e.g., water-level). Alternating thicknesses and apparent differences in erosional resistance has been suggested to reflect differential cementation (Cadieux & Kah, 2015). We suggest it may reflect the influence of the water level on different packages of strata or grain size. Our measurements do not show that bedding patterns reflect changes in orbital cycles (Lewis & Aharonson, 2014), although the regional trend may also reflect timing differences of deposition in different regions of AT as suggest recently by Annex & Lewis, 2020.

Lower deposit thickness within the Lower and Upper Mawrth groups might indicate the existence of high erosion rates unique to the northwest region of the study area. However, this assumes the Lower and Upper Mawrth craters were filled to the crater rims as observed in many craters of the Southern Region. We find this unlikely as yardangs are not a major feature of the Lower Mawrth ELDs. The two ELD mounds in Becquerel and Trouvelot are isolated and unique to the craters (Figure 6) and without the presence of other ELDs on the crater floors, there is no evidence that these craters once contained a larger crater-wide deposit. Furthermore, there are many craters of the Southern Region which contain ELDs of the same thickness as the Lower and Upper Mawrth craters (Table 2) which doesn't agree well with specific regional differences in erosion intensity as the major influence of ELD thickness. We also find it unlikely that every crater was completely filled to the rim and subsequently eroded to their present thicknesses because the ELDs within Firsoff and Crommelin are both as high as the crater rim. A scenario like this where one ELD can be completely eroded to something sparse, while others can remain as tall as the entire depth of the crater, requires drastically different erosion rates between craters of the same group and is thus not favorable.

Thus, while there are other variables to consider, it appears that latitude and elevation influences layer thickness more than anything else. However, it is unclear what the ratio of influence between latitude and elevation might have been for these deposits. Moreover, the existence of an ocean (Baker et al., 1991; Di Achille & Hynek, 2010) influencing the Upper and Lower Mawrth deposits could be a major factor as well. Elevation would be a major influence in terms of groundwater as the graph in Figure 9a combined with the putative long-term water level demonstrates and latitude would be a major influence in a dust rich atmosphere concentrated at the equator or a volcanic province ejecting ash from the south. However, the precise duality of water level and air fall is difficult to constrain if ELDs can be produced by fluid expulsion.

5.1.2. Layer Attitudes

Apart from the layer thickness trend, it is also observed a decrease in the *range* of layer thicknesses from southeast to northwest. A large range of layer thicknesses implies a more high energy or chaotic control(s) on deposition, which may be consistent with a proximal-distal relationship to the source but also with different depositional processes operating in different contexts.

ELDs show a wide variety of dip values and directions, but there are instances of individual craters having ELDs with unique dip values and preferred dip directions (Figure 10). Layer attitudes are significantly more complicated than those measured in Valles Marineris (Fueten et al., 2008, 2010, 2014, 2017; Schmidt et al., 2018) where dips rarely exceed 20° (Okubo et al., 2008) (e.g., Figure 5d). Folding is much more common in these ELDs and those observed in this study are much tighter compared to those presented in Schmidt et al. (2018) from Valles Marineris. There are many locations where dips are above the angle of repose for material with a grain size that could be transported by air or deposited by fluid-expulsion [34° from Atwood-Stone & McEwen (2013)] (Figure 10). Although there are many factors that contribute to the angle of repose (e.g., grain shape and moisture content) (Al-Hashemi & Al-Amoudi, 2018) we interpret high dips and localized preferred dip directions as reflective of each crater having either a unique post-depositional history, a pre-existing topography that influenced layer attitudes (for dips <34°), or a combination of the two. Thus, many of the higher dips might represent intense deformation that was localized to certain

individual craters, or possibly indicate regional compression (e.g., Danielson, Firsoff, Sera, Becquerel, and Becquerel B). Low dip values (below the angle of repose) might occur when layers were draped over a preexisting topography during deposition as described in Schmidt et al. (2018). Fold hinges parallel to crater rims could represent draping over secondary rims. Sets of parallel fold hinges could represent local faulting that produced enough vertical offset prior to deposition to create a pre-existing topography. Dip frequency shows that craters such as Becquerel and Danielson are particularly unique in this regard and are interpreted as having post-depositional deformational events as a major influence in high dips (Figures 5d and 6b). Such events could include subsidence, loss of volume from the dissolution of salts, or fluid pressure if springs were present below. Therefore, although layer thicknesses follow the southeast-northwest trend, layer attitudes have the tendency to be more unique to each crater while showing a lesser southeast-northwest trend.

Layer attitudes and folding could have formed syndepositionally or after deposition. Syndepositional-derived dip values roughly corresponding or exceeding the angle of repose of the materials might be related to syndepositional gravitative process (e.g., clinoforms) or syndepositional cementation (e.g., fluid expulsion) respectively. Post-depositional dip values might derive from sliding along the crater walls or topographic irregularities, or differential compaction. Faulting, generally characterized by high-angle and limited offsets, is locally diffuse, and there are deposits with little to no observed faulting in close vicinity to deposits with extreme faulting (e.g., Jiji versus Danielson or Trouvelot versus Becquerel). Subsidence may have lowered the crater floors unevenly and produced folding structures, however many of the folds are observed in areas close to the crater rim and in relatively thin deposits, suggesting the importance of sliding along the crater walls. We argue that many of the measured high dip values and chaotic dip directions pose challenges for the katabatic wind hypothesis (Kite et al., 2013) if they are syndepositional.

Subsidence may have had a role in layer thickness variations because complex craters have a period of collapse and even uplift after impact. However, the timescale of crater collapse is generally thought to be shorter in comparison with the accumulation rate of sediments (Melosh and Ivano, 1999). Additionally, it is unlikely that numerous craters would be undergoing the same stage of early formation at the same time. Thus, while subsidence may not describe the regional layer thickness trend, it might explain thickening upwards trends and folding within individual craters.

5.1.3. Crater Group Relationships

The Upper Mawrth crater group is unique in that it is the only group to have isolated ELD mounds. The similar layer thickness average of the ELDs within Becquerel and Trouvelot, coupled with their isolated, off-centered spatial positions on the crater floors (Figure 6), suggests these are of a shared environment either from being fringe deposits from the extent of deposition favored the Southern Region craters, or they are a separate deposition entirely.

Based on layer thicknesses, the ELD within Becquerel B is more closely related to those of the Lower Mawrth crater group, although geographically grouped with the Upper Mawrth crater group. Since Becquerel B has a similar elevation to the Lower Mawrth group, these layer thicknesses are evidence of the existence of the long-term −4,000-m water level which could influence the formation of thinner layers. However, since Becquerel B has some of the highest dips measured in this study, it had a unique post-depositional process not undergone by the Lower Mawrth deposits. Lower Mawrth deposits are a mix of eroded crater floor and subsequent alteration, shoreline levels that create the illusion of layering, and clays as observed nearby in Mawrth Vallis (Loizeau et al., 2012). Small craters in the floor of Oyama for example show layering in the crater wall implying that the crater floor itself is layered. However, there are layered conical buttes in both Oyama and McLaughlin that are very similar to those observed in the Southern Boundary craters such as Jiji South, Sera, and Vernal (Figure 5a), implying a similar erosional process took place across the study area akin to the process described in Franchi et al. (2020), which proposes that these features are points of higher erosional resistance due to compositional changes caused by capillary forces located beneath them.

It is also proposed that our measurements from Kotido (1.49 m avg. layer thickness) represent a unit related to a stratigraphic section originally discovered in Crommelin by the measurements of Lewis and Aharonson (2014) (2.5-m avg. layer thickness). They are both likely from a later deposition that created a veneer on the flanks of Crommelin's ELD mound and filled the floor of an empty Kotido. These could represent

changing conditions from a groundwater upwelling/evaporation setting to a lacustrine setting if a crater was able to sustain standing water for a period of time and form thinner layers.

5.2. Garvin Power Law

The majority of craters have large differences between their measured crated depth and Garvin power law derived crater depth (Table 2). On average, the total calculated difference was 492 m (Southern Region = 730 m, Upper Mawrth = 174 m, Lower Mawrth = 513) and indicates the possibility that craters can be deeper than measurable due to infill covering the crater floor. This means that some of these craters have significant sections of buried ELD. For example, Firsoff and Vernal craters have Garvin depths of 1,318 and 1,570 m respectively, deeper than their measured depths (Table 2). As demonstrated previously by Franchi et al. (2014), these values might indicate that the true thickness of the deposit is the combined measurable deposit thickness and Garvin depth. Conversely, Trouvelot and Rutheford crater have Garvin depths 743 and 612 (respectively) *shallower* than the measured depth (Table 2). This might indicate a unique erosional process which excavated part of the crater floor, or that the crater floor underwent partial collapse. Since Trouvelot and Rutherford do not have very exceptionally large deposits, we find subsidence induced from weight load of the ELD to be unlikely. However, deep sections of crater floor may have formed from local collapse, perhaps due to groundwater upwelling or loss of volume below the surface.

5.3. ELD Deposition

5.3.1. Aeolian Deposition

The presented regional study provides insights into possible processes and controls for ELD deposition. ELDs may source from above (air fall and/or pyroclastic) (Annex & Lewis, 2020; Bennett & Bell, 2016; Cadieux & Kah, 2015; Kite et al., 2013; Le Deit et al., 2013, Lewis & Aharonson et al., 2014; Michalski & Niles, 2012; Zabrusky et al., 2012), from surficial drainage, either of fluvio-lacustrine or glacial (Day et al., 2019; Fueten et al., 2017; Niles & Michalski, 2009) or from subsurface through fluid upwelling (i.e., subsurface-fed lakes: Salese et al., 2019) fluid expulsions processes (e.g., Allen & Oehler, 2008; Pondrelli et al., 2015, 2019; Pozzobon et al., 2019; Rossi et al., 2008) or diapirism (Jackson et al., 2011). Separate from the other processes, groundwater upwelling might also contribute to ELD preservation by promoting diagenetic processes able to harden the deposits and preserving them from the following erosion as observed for example in Meridiani Planum (e.g., Grotzinger et al., 2005). Moreover, all ELDs were not necessarily produced by a single depositional process.

Aeolian deposition, particularly by ash fall or dust, is an attractive solution for explaining many of the observations (Annex & Lewis, 2020; Kite et al., 2016, 2013; Lewis & Aharonson et al., 2014; Hayes et al., 2011). Also, layer thicknesses and layer uniformity resemble somewhat ILDs studied in VM which have previously been proposed to have formed from aeolian deposition (Fueten et al., 2014; Kite et al., 2016; Schmidt et al., 2018). In general, the thickness of an ash deposit decreases as distance from the source increases, which can explain the observed basin and layers thickness trends if a volcanic province to the east such as Syrtis Major (3,500 km east) is the ash source (Fassett & Head, 2007). Depositional geometry would be consistent since most of the deposits appear to drape the original topography only rarely exceeding the angle of repose. Formation of hydrated minerals from volcanic ash has been proposed previously in Meridiani Planum (McCollom & Hynek, 2005) and fits into an ash origin of these deposits as well.

Deposition by air fall (either dust or ash) has several problems, most of which stem from deposits being present in less than 10% of the craters (Figure 1). This may be a factor of age if featureless craters represent impacts that happened after the depositional period. However, older craters are typically those with larger diameter, and our measurements showed that crater diameter does not influence the likelihood of it containing a deposit, only that larger diameter favors a thicker deposit. The relationship between large diameter craters and thicker deposits is likely due to the depth of penetration also being larger, thus there is more accommodation space for a deposit. ELDs display aeolian erosional features and are generally thought to be more extensive in the past (Zabrusky et al., 2012). However how much more extensive these deposits were is a fundamental question still debated. It is often suggested that layered deposits within craters and layered deposits on the plateau share the same depositional method (Bennett & Bell, 2016). Layered deposits are

prolific on the plateau of Meridiani Planum and although they are not as common in AT, the ELDs tend to have the general appearance of being separate from them (Flahaut et al., 2015; Pondrelli et al., 2015). If all the Southern Region craters (Figure 4) were completely filled from ash fall or dust, we can approximate the minimum volume of material required by using the group's average crater dimension (Table 2), solving for the volume of a half ellipsoid, and then multiplying that by the number of craters in the group (24):

$$v = \frac{\left(\frac{4}{3} \cdot \pi \cdot d \cdot r1 \cdot r2\right)}{2} \cdot 24$$

The volume of material required is over 23,000 km^3 and is compounded if deposition continues to also cover the plateau. Moreover, combining explanations of how this material is eroded and where it is transported creates a very unrealistic setting. Even the largest volumes of single deposits of ash on Earth do not exceed 10,000 km^3 (Bryan et al., 2010). Perhaps many separate eruptions occurred and were part of a long duration of volcanic activity in which ash did not fill the craters entirely and were only deposited on the plateau in sporadic patches. The Syrtis Major volcanic province makes a strong candidate for the location of such eruptions, however based on pyroclastic ejecta modeling, ash from Syrtis Major would not have been distributed in the study area (Kerber et al., 2012). In order to refine the ash fall origin hypothesis, modeling predictions must coincide with these craters, or an undiscovered buried volcanic province is the source. The supervolcanoes proposed by Michalski and Bleacher (2013) are not suitable candidates for the source of these deposits because their northwest location would not lead to the regional trends presented in this work.

To counter ash as a source, a blanketing air fall scenario recently proposed by Annex and Lewis (2020) for craters in this area argues dust accumulation. However, this depositional hypothesis also fails to address the existence of many featureless and flat-floor craters adjacent to those with LEDs. It is claimed that modern dust accumulation rates can account for the infill of the nine craters in the study, but does not explain why craters such as Danielson, Firsoff, and Crommelin have deposits with thicknesses of 1,575, 1,716, and 2,145 m, respectively, but craters such as Becquerel, Trouvelot, Kotido, Sera, Jiji and others do not even reach 500 m in thickness. If the wind itself is the driving force of sedimentation, as proposed by Kite et al. (2013), then presumably wind direction is the reason of such differing spatial position geometries mentioned earlier, but this does not explain the presence of completely different depositional geometries and morphological association. Groundwater-driven cementation might have led to the preservation of more materials inside the deepest craters. However the amount of necessary erosion, the presence of randomly located featureless craters, and the association of the ELD with different morphologies suggest that dust and/or pyroclastic deposition, might have been part of the depositional processes, but are unlikely to have been the only process leading to ELD deposition.

5.3.2. Lacustrine Deposition and Water Level

While no major regional drainage and associated crater breaches were found to constrain a lacustrine deposition fed by surficial drainage(Annex & Lewis, 2020; Pondrelli et al., 2015, 2019; Salese et al., 2019), lacustrine deposition may fit well with the observations, if the lake depth was dependent on a fluctuating regional water-table. Generally, changes in water level followed by periods of stability might reflect the changing thicknesses with elevation. Thinning and thickening sequences could be a reflection of different depositional trends of lacustrine deposition reflecting different ratio between accommodation space and accumulation rate. Lacustrine systems might be either clastic- or evaporite-dominated systems. Clastic deposition should be associated to sapping channels along the crater rims debouching in the standing body of water through deltas, and all related morphologies/environments (e.g., terraces and channels). This morphofacies association is present in the Lower Mawrth craters (Salese et al., 2019), and locally in the Upper Mawrth craters (e.g., in Bequerel B), but becomes absent moving southeastward to the Southern Region craters. This distribution corresponds roughly to an elevation of the top of such deposits between −3500 and −4000 m below Mars datum, that correspond to the groundwater level inferred by Salese et al. (2019). Similar observations within McLaughlin crater have also been proposed to represent a water level at an average elevation of −4,635 m (Michalski et al., 2019). This provides strong evidence for the interaction of water and these deposits. Even if deposited into dry craters, this water level may have fluctuated enough to

influence their lithification and alteration. Lithification is likely the result of a cementation from chemical precipitation in pore space from water.

Evaporite-dominated lacustrine systems would reflect water upwelling and almost immediate precipitation from an ephemeral body of water (i.e., playa) or in association with aeolian deposition as evaporative pumping in the capillary zone (i.e., sabkha). Many deposits display superimposed mounds 50–300 m in diameter and are strong candidates for the deposition of material by groundwater activity (Franchi et al., 2014; Pondrelli et al., 2015, 2011, 2019; Pozzobon et al., 2019). They are often in collinear groups where escaping water might take advantage of a pre-existing fault or less resistant layer (Allen & Oehler, 2008; Pozzobon et al., 2019). The ELDs generally display uniform and lateral continuous layering that could not be produced by these smaller conical mound producing springs. Grindrod and Balme (2010) demonstrated that if water upwelling created the >7 km high layered mound within Hebes Chasma, it would have required an unrealistic pressure gradient to reach the higher elevations of a layered mound. This suggests a strong upwelling force would also be needed for water to penetrate the ELDs and form conical mounds on top. However, since the ELDs examined in our study area only once exceed 2 km in height (Crommelin), the high pressure required is less of a problem than in Hebes Chasma. At a minimum, it is likely that groundwater influenced ELD lithification and alteration in a type of sabkha or playa condition (Day et al., 2019).

However, lakes as a depositional method do not explain layer attitudes, plateau deposits, and deposits observed in several craters where layering exists at elevations at or just below the elevation of the crater rim. It is possible ELDs were deposited by a different method, but then lakes contributed to their alteration. Equally, upwelling groundwater may have deposited the ELDs while simultaneously filling the craters with deep standing water. Thus, craters at higher elevations may have been more susceptible to water level changes, whereas craters at lower elevations remained submerged more often. In this scenario, it is possible that changing layer thicknesses represent changing accommodation space due to constantly changing water depth. Groundwater activity sourced at the Meridiani-Arabia boundary is reinforced by global hydrology modeling (Andrews-Hanna et al., 2007) and the regional thickness trend may indicate that deposition is influenced by the proximity to Meridiani Planum. However, one problem with this is the presence of ELDs in Henry and other craters in the east (longitudes 10°–20° in Figure 2), which are some of the largest layered mounds in AT. These ELDs are much further away from Meridiani Planum, which might suggest that groundwater activity is not strictly sourced to a particular location and could be more widespread (Salese et al., 2019).

Considerable discussion exists in the literature about the nature of lacustrine deposits versus ash fall deposits versus spring mounds, however the ability for all three processes to have coexisted has yet to be appreciated. It is unclear if some of the spring mounds presented by Allen and Oehler (2008), Franchi et al. (2014), Pondrelli et al. (2011, 2015, 2019), and Pozzobon et al. (2019), and are just heavily eroded portions of once united ELD and their layering indistinguishable, creating the illusion of a layerless mound separate from the ELD (Figure 5b). If we assume these mounds are erosional features of a once larger ELD, a discussion should at least attempt to address what process erodes infilled craters in this manner. Perhaps the process invoked by Franchi et al. (2020), where the layered conical mounds represent points of higher erosional resistance due to capillary forces beneath them, could also produce collinear groups of mounds (Allen & Oehler, 2008) if the increased capillary force was following faults. In addition, it isn't obvious that the ELD literature of AT is referencing all the features correctly in the debate of spring mounds versus long continuous layers filling craters. Without a credible erosional process, mounds weathered from air fall deposits (dust or ash) is problematic. These mounds are not streamlined and they are devoid of yardangs, making a wind erosion difficult to argue. It is also unlikely that kilometers of continuous layering can by produced by a single spring. Furthermore, it has already been established by Grindrod and Balme (2010) that thick deposits might not be produced solely from groundwater upwelling due to unrealistic water pressure gradients.

5.3.3. Diapirs, Dusty Glaciers, and Lava

We found that several previously proposed depositional methods do not explain well the observed regional trend. Diapiric uplift, although might be argued locally within craters with isolated mounds (e.g., Becquerel and Trouvelot), does not match well with the observed complexity of the regional basin and layer thicknesses trends. The lack of glacial morphology does not fit well with a dusty glacier scenario (Niles & Michalski, 2009). Although the layer thickness trend could be tied to the deposition of northward receding

glaciers, it requires continual, repeated glaciations to deposit individual layers. A period of seasonal stability to maintain such repeated glaciations has been suggested previously and linked to obliquity changes (Lewis & Aharonson, 2014; Niles & Michalsk, 2009), however the spatial positions of the deposits are too chaotic and do not align in a northward direction as would be expected. A lava flow origin for these deposits, as proposed for some layered plateau deposits around VM (Leone, 2014) and in Meridiani Planum (Hynek et al., 2002), does not fit well with observations. These deposits lack flow structures. Furthermore, continuous layering across tens to hundreds of kilometers is implausible if each layer represented a separate lava flow. It is also difficult to reconcile lava flows with the perceived rhythmic bedding (Cadieux & Kah, 2015; Lewis & Aharonson, 2014) within packages of some sections. Furthermore, the rims of these craters lack geomorphological evidence of lava that poured from the plateau. That being said, the "flat-floor craters" presented in Figures 2b and 3a probably represent a lava infill.

5.4. Alteration

Although no mineralogical data is presented in this study, the mineralogy of layered deposits presented in previous studies (Andrews-Hanna et al., 2010; Loizeau et al., 2012, 2015; McKeown et al., 2009; Michalski et al., 2019; Zabrusky et al., 2012), shows clays constitute the majority of the deposits in the northwestern area and hydrated sulfates seem to be associated with larger mounds in the southeast. This change is likely tied to the regional layer thickness trend and invokes the idea of a regional facies change. Perhaps clays tend to form at lower elevations due to a relationship with water level or the formation of hydrated sulfates is the product of water from a different source. The water source in the southeast would have then been more sulfur rich or deposits compositionally had more sulfur than in the northwest. It is unclear whether the clays and hydrated sulfates are coeval, but alternating units observed in Gale Crater (Thomson et al., 2011) and Meridiani Planum (Flahaut et al., 2015) suggests they are different ages.

The Compact Reconnaissance Imaging Spectrometer (CRISM) has detected a vast expanse of hydrated minerals across the mapping area. In the northwest, Mawrth Vallis has shown predominately clays (Loizeau et al., 2012, 2015) as well as Mclaughlin Crater (McKeown et al., 2009; Michalski et al., 2019). Further southeast, analyses have detected hydrated sulfates associated with ELDs at the boundary between AT and Meridiani Planum (Andrews-Hanna et al., 2010; Zabrusky et al., 2012), as well as a mix of both hydrated sulfate and clay units in Meridiani Planum (Flahaut et al., 2015). Unfortunately, most CRISM observations of ELDs in AT are impeded by a fine layer of dust (Allen & Oehler, 2008; Zabrusky et al., 2012), thus no extensive CRISM analysis has been published on these deposits. Among similar deposits outside of AT, CRISM analyses have shown the presence of alternating units of clay and hydrated sulfates in Aeolis Mons inside Gale crater (Thomson et al., 2011) and predominately hydrated sulfates with smaller areas of mixed clays in the ILD mounds of VM (Fueten et al., 2014; Schmidt et al., 2018). This scale of hydrated alteration likely required the stability of liquid water at the surface and thus occurred during a time when the atmosphere was much thicker.

6. Conclusions

We conclude that a unified depositional method of ELDs in AT does not fit the full range of data and observations presented here. Furthermore, post-depositional histories are often drastically different between ELDs which have created unique deformational features, as well as deposit forms and shapes.

Putative super volcanoes in the northwest such as Eden Patera are not sources for any of these deposits. An origin as dust deposits eliminates the need for a volcanic province, but could require periods of equatorial dust saturation. Equatorial atmospheric dust saturation could explain the regional deposit thickness trend, however it does not explain the large number of craters without an ELD. The existence of many featureless craters and the diverse spatial placement of ELDs within craters remain significant problems. The absence of yardangs on most of these deposits negates the fact they have low retention ages, and when combined with the craters without ELDs, shows that not all craters present at the time of deposition necessarily had an ELD that was eroded away. Furthermore, dust deposits of non-glacial loess on Earth do not form layering, thus a control is required that regulates layer formation and layer thickness. Controls could be periods of high and low atmospheric dust saturation, particle size, and water level present within a crater at the time

of the formation of a layer are all possible controls to the formation of layering. The long term water level elevation of −4,000 m can be used to separate the existence of thicker layers from craters only containing thinner layers, which further supports the existence of a northwest-southeast facies change. It does not mean that the higher Southern Region ELDs were deposited into dry craters. Many aspects of their layer structure and alteration imply water interaction or even deposition into standing water. Furthermore, deposition into dry craters would be unlikely given their proximity to the intense aqueous history of Meridiani Planum. Due to their off-center spatial placement, the two ELD mounds in Trouvelot and Becquerel may very well be the result of fluid expulsion or even salt diapirism, or at the least a much different wind pattern within the crater than those in the Southern Region.

Apart from deposition, groundwater activity associated with Meridiani Planum may have contributed much to the post-depositional environment by influencing the lithification and alteration of the ELDs. Upwelling may have been influenced by a fluctuating regional water table that contributed to periods of standing water within craters. This would have left craters at lower elevations submerged more often than those at higher elevations. Large ranges of layer thicknesses at higher elevations reflect the high energy conditions produced in such a scenario (Schmidt et al., 2018). Additionally, groundwater behavior may be influenced by differences in lithology and the amount of faults. A later deposition of ground water upwelling produced the small conical mounds that are superimposed on the older deposits (Figure 5b). Conical mounds are features commonly discussed associated with some of the ELDs of the Southern Region craters, yet are are not observed in all ELD bearing craters. This suggests their occurrence is more exclusive to the conditions of individual craters, rather than whole groups of craters. It also suggests they are younger. However, their formation mechanism may still represent a process which influenced ELD deposition.

Comparisons between layer thickness measurements on the ELDs in AT (this study as well as others) and those done previously on the ILDs in VM (Annex & Lewis, 2020, Fueten et al., 2014, 2017; Lewis & Aharonson, 2014; Schmidt et al., 2018), at this point suggests that ILDs and ELDs were produced from separate depositional events, or from a shared global event where conditions favored thicker layering in VM (e.g., distance to source or speed of deposition vs. water level). In VM layering thins upwards in elevation, whereas in AT layering thickens upwards in elevation (Fueten et al., 2014; Schmidt et al., 2018). However, due to their overwhelming similarity, the depositional processes are likely similar and the high energy environment that produced thicker layering in ILDs and ELDs may have endured in both regions simultaneously.

Further analysis of the layer thicknesses of these deposits may reveal thickening and thinning sequences shared between localized craters that may represent a shared sedimentary unit, as proposed by Annex and Lewis (2020) to exist in several craters. Similar measurements must also be attempted in craters further east, however higher amounts of dust covering these deposits causes thinner layering to be observed which reduces the reliability of layer thickness measurements obtained from them. Arguably the largest downfall of this work is that HiRISE stereo pairs are not available for every deposit found, thus the presented data does not represent the complete character of these deposits and their regional relationships. Thus, more high resolution stereo imagery is needed to acquire a complete and comprehensive stratigraphic succession of these deposits.

Future work includes constraining lateral fluctuations of layer thicknesses of certain deposits, determining timing of folding and faulting, and analyzing deposits for unconformities within ELDs as observed in VM (Fueten et al., 2017; Schmidt et al., 2018) which can help to indicate interval periods in deposition. Future work must be done to characterize the nomenclature of ELDs, ILDs, LTD/LLDs, intracrater deposits, and plateau deposits so that we can move forward with a clear and universal definition of when they should be applied. Future work should also attempt to differentiate the ages of craters in AT so it can be reliably understood which craters existed at the time of ELD deposition and which did not. Lastly, work to constrain the possibility that the three groups represent three different zones of alteration is needed.

Data Availability Statement

All of the HiRISE, CTX, and HRSC data used in this study are available from the Planetary Data System (PDS) node at their respective archives listed and linked here: https://pds.nasa.gov/datasearch/subscription-service/SS-20150302.shtml (Malin et al., 2007b; McEwen et al., 2005; McEwen 2006; McEwen &

Team, 2009) and https://www.cosmos.esa.int/web/psa/mars-express (Heather et al., 2013a, 2013b). Satellite imagery and topography were processed in-house with ISIS (Integrated Software for Imagers and Spectrometers) available online at https://isis.astrogeology.usgs.gov. Processed data was projected into a Global Mapper 15.0 GIS software environment. Data for this work is publicly available at: https://doi.org/10.5281/zenodo.5150395 (Schmidt, 2021).

Acknowledgments
We would like to thank Dr. Jessica Flahaut for many conversations about ELDs in Arabia Terra. We would like to acknowledge Dr. Gerhard Neukum and the HRSC Science Team for the joint effort in processing the HRSC DEM of the MC-11 quadrangle of Mars. We also thank Adriano Tullo for script advice and helping process several of the HiRISE DEMs. F. Salese is supported by "MarsFirstWater," funded by the European Research Council, Consolidator Grant 818602 (P. I. Alberto G. Fairén). This work was funded by GeoQuTe Lab (Laboratorio di Geodinamica Quantitativa *e* Telerilevamento) of Roma Tre University.

References

Al-Hashemi, H. M. B., & Al-Amoudi, O. S. B. (2018). A review on the angle of repose of granular materials. *Powder Technology*, *330*, 397–417. https://doi.org/10.1016/j.powtec.2018.02.003

Allen, C. C., & Oehler, D. Z. (2008). A case for ancient springs in Arabia Terra, Mars. *Astrobiology*, *8*(6), 1093–1112. https://doi.org/10.1089/ast.2008.0239

Al-Samir, M., Nabhan, S., Fritz, J., Winkler, A., Bishop, J. L., Gross, C., & Jaumann, R. (2017). The paleolacustrine evolution of Juventae Chasma and Maja Valles and its implications for the formation of interior layered deposits on Mars. *Icarus*, *292*, 125–143. https://doi.org/10.1016/j.icarus.2016.12.023

Andrews-Hanna, J. C., Zuber, M. T., Arvidson, R. E., & Wiseman, S. M. (2010). Early Mars hydrology: Meridiani playa deposits and the sedimentary record of Arabia Terra. *Journal of Geophysical Research*, *115*(E6). https://doi.org/10.1029/2009JE003485

Andrews-Hanna, J. C., Phillips, R. J., & Zuber, M. T. (2007). Meridiani Planum and the global hydrology of Mars. *Nature*, *446*(7132), 163–166. https://doi.org/10.1038/nature05594

Annex, A. M., & Lewis, K. W. (2020). Regional correlations in the layered deposits of Arabia Terra, Mars. *Journal of Geophysical Research: Planets*, *125*(6), e2019JE006188. https://doi.org/10.1029/2019JE006188

Ansan, V., Loizeau, D., Mangold, N., Le Mouélic, S., Carter, J., Poulet, F., et al. (2011). Stratigraphy, mineralogy, and origin of layered deposits inside Terby crater, Mars. *Icarus*, *211*(1), 273–304. https://doi.org/10.1016/j.icarus.2010.09.011

Arvidson, R. E., Poulet, F., Bibring, J. P., Wolff, M., Gendrin, A., Morris, R. V, et al. (2005). Spectral reflectance and morphologic correlations in eastern Terra Meridiani, Mars. *Science*, *307*(5715), 1591–1594. https://doi.org/10.1126/science.1109509

Atwood-Stone, C., & McEwen, A. S. (2013). Avalanche slope angles in low-gravity environments from active Martian sand dunes. *Geophysical Research Letters*, *40*(12), 2929–2934. https://doi.org/10.1002/grl.50586

Baker, V. R., Strom, R. G., Gulick, V. C., Kargel, J. S., Komatsu, G., & Kale, V. S. (1991). Ancient oceans, ice sheets and the hydrological cycle on Mars. *Nature*, *352*(6336), 589–594. https://doi.org/10.1038/352589a0

Bennett, K. A., & Bell, J. F., III (2016). A global survey of Martian central mounds: Central mounds as remnants of previously more extensive large-scale sedimentary deposits. *Icarus*, *264*, 331–341. https://doi.org/10.1016/j.icarus.2015.09.041

Bibring, J. P., Langevin, Y., Mustard, J. F., Poulet, F., Arvidson, R., Gendrin, A., et al. (2006). Global mineralogical and aqueous Mars history derived from OMEGA/Mars express data. *Science*, *312*, 400–404. https://doi.org/10.1126/science.1122659

Bishop, J. L., Gross, C., Danielsen, J., Parente, M., Murchie, S. L., Horgan, B., et al. (2020). Multiple mineral horizons in layered outcrops at Mawrth Vallis, Mars, signify changing geochemical environments on early Mars. *Icarus*, *341*, 113634. https://doi.org/10.1016/j.icarus.2020.113634

Bishop, J. L., Dobrea, E. Z. N., McKeown, N. K., Parente, M., Ehlmann, B. L., Michalski, J. R., et al. (2008). Phyllosilicate diversity and past aqueous activity revealed at Mawrth Vallis, Mars. *Science*, *321*(5890), 830–833. https://doi.org/10.1126/science.1159699

Blue Marble Geographics (2011). Global Mapper [computer software].

Bryan, S. E., Peate, I. U., Peate, D. W., Self, S., Jerram, D. A., Mawby, M. R., et al. (2010). The largest volcanic eruptions on Earth. *Earth-Science Reviews*, *102*(3–4), 207–229. https://doi.org/10.1016/j.earscirev.2010.07.001

Cadieux, S. B., & Kah, L. C. (2015). To what extent can intracrater layered deposits that lack clear sedimentary textures be used to infer depositional environments? *Icarus*, *248*, 526–538. https://doi.org/10.1016/j.icarus.2014.11.004

Carr, M. H., & Head, J. W., III (2010). Geologic history of Mars. *Earth and Planetary Science Letters*, *294*(3–4), 185–203. https://doi.org/10.1016/j.epsl.2009.06.042

Carter, J., Poulet, F., Bibring, J. P., Mangold, N., & Murchie, S. (2013). Hydrous minerals on Mars as seen by the CRISM and OMEGA imaging spectrometers: Updated global view. *Journal of Geophysical Research: Planets*, *118*(4), 831–858. https://doi.org/10.1029/2012JE004145

Catling, D. C., Wood, S. E., Leovy, C., Montgomery, D. R., Greenberg, H. M., Glein, C. R., & Moore, J. M. (2006). Light-toned layered deposits in Juventae Chasma, Mars. *Icarus*, *181*(1), 26–51. https://doi.org/10.1016/j.icarus.2005.10.020

Christensen, P. R., Morris, R. V., Lane, M. D., Bandfield, J. L., & Malin, M. C. (2001). Global mapping of Martian hematite mineral deposits: Remnants of water-driven processes on early Mars. *Journal of Geophysical Research*, *106*(E10), 23873–23885. https://doi.org/10.1029/2000JE001415

Coles, K., Tanaka, K., & Christensen, P. (2019). Arabia (MC-12). In *The atlas of Mars: Mapping its geography and geology* (pp. 132–135). Cambridge University Press. https://doi.org/10.1017/9781139567428.017

Day, M., Anderson, W., Kocurek, G., & Mohrig, D. (2016). Carving intracrater layered deposits with wind on Mars. *Geophysical Research Letters*, *43*(6), 2473–2479. https://doi.org/10.1002/2016GL068011

Day, M., Edgettm, K. S., & Stumbaugh, D. (2019). Ancient stratigraphy preserving a wet-to-dry, fluvio-lacustrine to aeolian transition near Barth crater, Arabia Terra, Mars. *Journal of Geophysical Research: Planets*, *124*(12), 3402–3421. https://doi.org/10.1029/2019je006226

Di Achille, G., & Hynek, B. M. (2010). Ancient ocean on Mars supported by global distribution of deltas and valleys. *Nature Geoscience*, *3*(7), 459–463. https://doi.org/10.1038/ngeo891

Evans, A. J., Andrews-Hanna, J. C., & Zuber, M. T. (2010). Geophysical limitations on the erosion history within Arabia Terra. *Journal of Geophysical Research*, *115*(E5). https://doi.org/10.1029/2009JE003469

Fassett, C. I., & Head, J. W., III (2007). Layered mantling deposits in northeast Arabia Terra, Mars: Noachian-Hesperian sedimentation, erosion, and terrain inversion. *Journal of Geophysical Research*, *112*(E8). https://doi.org/10.1029/2006JE002875

Fergason, R. L., & Christensen, P. R. (2008). Formation and erosion of layered materials: Geologic and dust cycle history of eastern Arabia Terra, Mars. *Journal of Geophysical Research*, *113*(E12). https://doi.org/10.1029/2007JE002973

Flahaut, J., Carter, J., Poulet, F., Bibring, J. P., Van Westrenen, W., Davies, G. R., & Murchie, S. L. (2015). Embedded clays and sulfates in Meridiani Planum, Mars. *Icarus*, *248*, 269–288. https://doi.org/10.1016/j.icarus.2014.10.046

Franchi, F., MacKay, R., Selepeng, A. T., & Barbieri, R. (2020). Layered mound, inverted channels and polygonal fractures from the Makgadikgadi pan (Botswana): Possible analogues for Martian aqueous morphologies. *Planetary and Space Science*, *192*, 105048. https://doi.org/10.1016/j.pss.2020.105048

Franchi, F., Rossi, A. P., Pondrelli, M., & Cavalazzi, B. (2014). Geometry, stratigraphy and evidences for fluid expulsion within Crommelin crater deposits, Arabia Terra, Mars. *Planetary and Space Science*, *92*, 34–48. https://doi.org/10.1016/j.pss.2013.12.013

Fueten, F., Flahaut, J., Stesky, R., Hauber, E., & Rossi, A. P. (2014). Stratigraphy and mineralogy of Candor Mensa, west Candor Chasma, Mars: Insights into geologic history of Valles Marineris. *Journal of Geophysical Research: Planets*, *119*, 331–354. https://doi.org/10.1002/2013je004557

Fueten, F., Racher, H., Stesky, R., MacKinnon, P., Hauber, E., McGuire, P. C., et al. (2010). Structural analysis of interior layered deposits in Northern Coprates Chasma, Mars. *Earth and Planetary Science Letters*, *294*(3–4), 343–356. https://doi.org/10.1016/j.epsl.2009.11.004

Fueten, F., Novakovic, N., Stesky, R., Flahaut, J., Hauber, E., & Rossi, A. P. (2017). The evolution of Juventae Chasma, Valles Marineris, Mars: Progressive collapse and sedimentation. *Journal of Geophysical Research: Planets*, *122*(11), 2223–2249. https://doi.org/10.1002/2017JE005334

Fueten, F., Stesky, R., MacKinnon, P., Hauber, E., Zegers, T., Gwinner, K., et al. (2008). Stratigraphy and structure of interior layered deposits in west Candor Chasma, Mars, from high resolution stereo camera (HRSC) stereo imagery and derived elevations. *Journal of Geophysical Research*, *113*(E10). https://doi.org/10.1029/2007JE003053

Garvin, J. B., Sakimoto, S. E., Frawley, J. J., & Schnetzler, C. (2000). North polar region craterforms on Mars: Geometric characteristics from the Mars Orbiter Laser Altimeter. *Icarus*, *144*(2), 329–352. https://doi.org/10.1006/icar.1999.6298

Garvin, J. B., Sakimoto, S. E. H. & Frawley, J. J. (2003). Craters on Mars: Global geometric properties from gridded MOLA topography. Sixth International Conference on Mars, 3277, 2003.

Gendrin, A., Mangold, N., Bibring, J. P., Langevin, Y., Gondet, B., Poulet, F., et al. (2005). Sulfates in Martian layered terrains: The OMEGA/Mars express view. *Science*, *307*(5715), 1587–1591. https://doi.org/10.1126/science.1109087

Gou, S., Yue, Z., Di, K., & Wang, J. (2014). Hyperspectral identification of mineral diversity and formation mechanism analysis in the Mclaughlin crater on Mars. In *Remote sensing of the environment: 18th national symposium on remote sensing of china* (Vol. 9158, p. 91580J). International Society for Optics and Photonics. https://doi.org/10.1117/12.2063744

Griffes, J. L., Arvidson, R. E., Poulet, F., & Gendrin, A. (2007). Geologic and spectral mapping of etched terrain deposits in northern Meridiani Planum. *Journal of Geophysical Research*, *112*(E8). https://doi.org/10.1029/2006JE002811

Grindrod, P. M., & Balme, M. R. (2010). Groundwater processes in Hebes Chasma, Mars. *Geophysical Research Letters*, *37*(13). https://doi.org/10.1029/2010GL044122

Grotzinger, J. P., Arvidson, R. E., Bell, J. F., III, Calvin, W., Clark, B. C., Fike, D. A., et al. (2005). Stratigraphy and sedimentology of a dry to wet eolian depositional system, burns formation, Meridiani Planum, Mars. *Earth and Planetary Science Letters*, *240*(1), 11–72. https://doi.org/10.1016/j.epsl.2005.09.039

Hartmann, W. K. (2005). Martian cratering 8: Isochron refinement and the chronology of Mars. *Icarus*, *174*(2), 294–320. https://doi.org/10.1016/j.icarus.2004.11.023

Hayes, A. G., Grotzinger, J. P., Edgar, L. A., Squyres, S. W., Watters, W. A., & Sohl-Dickstein, J. (2011). Reconstruction of eolian bed forms and paleocurrents from cross-bedded strata at Victoria Crater, Meridiani Planum, Mars. *Journal of Geophysical Research*, *116*(E7). https://doi.org/10.1029/2010JE003688

Heather, D., Barthelemy, M., Manaud, N., Martinez, S., Szumlas, M., Vazquez, J., & Osuna, P. (2013a). ESA's planetary science archive: Status, activities and plans. *European Planetary Science Congress*, *8*.

Heather, D., Barthelemy, M., Manaud, N., Martinez, S., Szumlas, M., Vazquez, J. L., & Osuna, P. (2013b). ESA's Planetary Science Archive: Status and Plans. In *EGU general assembly conference abstracts, EGU2013*, (pp. 9151).

Hynek, B. M., Arvidson, R. E., & Phillips, R. J. (2002). Geologic setting and origin of Terra Meridiani hematite deposit on Mars. *Journal of Geophysical Research*, *107*(E10), 18–21. https://doi.org/10.1029/2002JE001891

Jackson, M. P. A., Adams, J. B., Dooley, T. P., Gillespie, A. R., & Montgomery, D. R. (2011). Modeling the collapse of Hebes Chasma, Valles Marineris, Mars. *GSA Bulletin*, *123*(7–8), 1596–1627. https://doi.org/10.1130/b30307.1

Jaumann, R., Neukum, G., Behnke, T., Duxbury, T. C., Eichentopf, K., Flohrer, J., et al. (2007). The high-resolution stereo camera (HRSC) experiment on Mars Express: Instrument aspects and experiment conduct from interplanetary cruise through the nominal mission. *Planetary and Space Science*, *55*(7–8), 928–952. https://doi.org/10.1016/j.pss.2006.12.003

Kerber, L., Head, J. W., Madeleine, J. B., Forget, F., & Wilson, L. (2012). The dispersal of pyroclasts from ancient explosive volcanoes on Mars: Implications for the friable layered deposits. *Icarus*, *219*, 358–381. https://doi.org/10.1016/j.icarus.2012.03.016

Kite, E. S., Lewis, K. W., Lamb, M. P., Newman, C. E., & Richardson, M. I. (2013). Growth and form of the mound in Gale crater, Mars: Slope wind enhanced erosion and transport. *Geology*, *41*(5), 543–546. https://doi.org/10.1130/G33909.1

Kite, E. S., Sneed, J., Mayer, D. P., Lewis, K. W., Michaels, T. I., Hore, A., & Rafkin, S. C. (2016). Evolution of major sedimentary mounds on Mars: Buildup via anticompensational stacking modulated by climate change. *Journal of Geophysical Research: Planets*, *121*(11), 2282–2324. https://doi.org/10.1002/2016JE005135

Komatsu, G., Ori, G. G., Ciarcelluti, P., & Litasov, Y. D. (2004). Interior layered deposits of Valles Marineris, Mars: Analogous subice volcanism related to Baikal Rifting, Southern Siberia. *Planetary and Space Science*, *52*(1–3), 167–187. https://doi.org/10.1016/j.pss.2003.08.003

Lakdawalla, E. (2019). Similarities and differences in the landing sites of ESA's and NASA's 2020 Mars rovers. *Nature Astronomy*, *3*(3), 190–192. https://doi.org/10.1038/s41550-019-0727-x

Le Deit, L., Hauber, E., Fueten, F., Pondrelli, M., Rossi, A. P., & Jaumann, R. (2013). Sequence of infilling events in Gale Crater, Mars: Results from morphology, stratigraphy, and mineralogy. *Journal of Geophysical Research: Planets*, *118*(12), 2439–2473. https://doi.org/10.1002/2012JE004322

Leone, G. (2014). A network of lava tubes as the origin of Labyrinthus Noctis and Valles Marineris on Mars. *Journal of Volcanology and Geothermal Research*, *277*, 1–8. https://doi.org/10.1016/j.jvolgeores.2014.01.011

Lewis, K. W., & Aharonson, O. (2014). Occurrence and origin of rhythmic sedimentary rocks on Mars. *Journal of Geophysical Research: Planets*, *119*(6), 1432–1457. https://doi.org/10.1002/2013JE004404

Lewis, K. W., Aharonson, O., Grotzinger, J. P., Kirk, R. L., McEwen, A. S., & Suer, T. A. (2008). Quasi-periodic bedding in the sedimentary rock record of Mars. *Science*, *322*(5907), 1532–1535. https://doi.org/10.1126/science.1161870

Loizeau, D., Mangold, N., Poulet, F., Bibring, J. P., Bishop, J. L., Michalski, J., & Quantin, C. (2015). History of the clay-rich unit at Mawrth Vallis, Mars: High-resolution mapping of a candidate landing site. *Journal of Geophysical Research: Planets*, *120*(11), 1820–1846. https://doi.org/10.1002/2015JE004894

Loizeau, D., Mangold, N., Poulet, F., Ansan, V., Hauber, E., Bibring, J. P., et al. (2010). Stratigraphy in the Mawrth Vallis region through OMEGA, HRSC color imagery and DTM. *Icarus*, *205*(2), 396–418. https://doi.org/10.1016/j.icarus.2009.04.018

Loizeau, D., Werner, S. C., Mangold, N., Bibring, J. P., & Vago, J. L. (2012). Chronology of deposition and alteration in the Mawrth Vallis region, Mars. *Planetary and Space Science*, *72*(1), 31–43. https://doi.org/10.1016/j.pss.2012.06.023

Lowe, D. R., Bishop, J. L., Loizeau, D., Wray, J. J., & Beyer, R. A. (2020). Deposition of >3.7 GA clay-rich strata of the Mawrth Vallis Group, Mars, in lacustrine, alluvial, and aeolian environments. *GSA Bulletin*, *132*(1–2), 17–30. https://doi.org/10.1130/B35185.1

Lucchitta, B. K. (2010). Lakes in Valles Marineris. In N. A. Cabrol, & E. A. Grin (Eds.), *Lakes on Mars [book]* (pp. 111–161). Elsevier. https://doi.org/10.1016/b978-0-444-52854-4.00005-2

Lucchitta, B. K., Isbell, N. K., & Howington-Kraus, A. (1994). Topography of Valles Marineris: Implications for erosional and structural history. *Journal of Geophysical Research*, *99*(E2), 3783–3798. https://doi.org/10.1029/93JE03095

Malin, M. C., Bell, J. F., III, Cantor, B. A., Caplinger, M. A., Calvin, W. M., Clancy, R. T., et al. (2007a). Context Camera Investigation on board the Mars Reconnaissance Orbiter. *Journal of Geophysical Research*, *112*, E05s04. https://doi.org/10.1029/2006je002808

Malin, M. C., Bell, J. F., III, Cantor, B. A., Caplinger, M. A., Calvin, W. M., Clancy, R. T., et al. (2007b).*Camera Experiment Data Record Level 0 v1.0 [data Set]* (Vol. 112), E05s04. NASA Planetary Data System. https://doi.org/10.1029/2006je002808MROContext10.17189/1520266

Malin, M. C., & Edgett, K. S. (2000). Sedimentary rocks of early Mars. *Science*, *290*(5498), 1927–1937. https://doi.org/10.1126/science.290.5498.1927

Mandt, K. E., de Silva, S. L., Zimbelman, J. R., & Crown, D. A. (2008). Origin of the Medusae Fossae Formation, Mars: Insights from a synoptic approach. *Journal of Geophysical Research*, *113*(E12). https://doi.org/10.1029/2008JE003076

Mangold, N., Carter, J., Poulet, F., Dehouck, E., Ansan, V., & Loizeau, D. (2012). Late Hesperian aqueous alteration at Majuro crater, Mars. *Planetary and Space Science*, *72*(1), 18–30. https://doi.org/10.1016/j.pss.2012.03.014

Mangold, N., Adeli, S., Conway, S., Ansan, V., & Langlais, B. (2012). A chronology of early Mars climatic evolution from impact crater degradation. *Journal of Geophysical Research*, *117*(E4). https://doi.org/10.1029/2011JE004005

Mangold, N., Ansan, V., Masson, P., & Vincendon, C. (2009). Estimate of aeolian dust thickness in Arabia Terra, Mars: Implications of a thick mantle (>20 m) for hydrogen detection. *Géomorphologie: Relief, Processus, Environnement*, *15*(1), 23–32. https://doi.org/10.4000/geomorphologie.7472

McCollom, T. M., & Hynek, B. M. (2005). A volcanic environment for bedrock diagenesis at Meridiani Planum on Mars. *Nature*, *438*(7071), 1129–1131. https://doi.org/10.1038/nature04390

McEwen, A. (2006). The high resolution imaging science experiment (HiRISE) on Mars Reconnaissance Orbiter (MRO). In *36th COSPAR Scientific Assembly* (Vol. 36, p. 1096).

McEwen, A. S., & Team, H. (2009). Recent MRO/HiRISE discoveries on Mars. In *EGU general assembly conference abstracts* (p. 6434).

McEwen, A., Eliason, E., Bergstrom, J., Bridges, N., Hansen, C., Delamere, W. A., et al. (2005). MRO's High Resolution Imaging Science Experiment (HiRISE). In *AGU fall meeting abstracts* (Vol. 2005, pp. P23A–P0171).

McEwen, A. S., Eliason, E. M., Bergstrom, J. W., Bridges, N. T., Hansen, C. J., Delamere, W. A., et al. (2007). Mars Reconnaissance Orbiter's High Resolution Imaging Science Experiment (HiRISE). *Journal of Geophysical Research*, *112*, E05s02. https://doi.org/10.1029/2005je002605

McKeown, N. K., Bishop, J. L., Noe Dobrea, E. Z., Ehlmann, B. L., Parente, M., Mustard, J. F., et al. (2009). Characterization of phyllosilicates observed in the central Mawrth Vallis region, Mars, their potential formational processes, and implications for past climate. *Journal of Geophysical Research*, *114*(E2). https://doi.org/10.1029/2008JE003301

Melosh, H. J., & Ivanov, B. A. (1999). Impact crater collapse. *Annual Review of Earth and Planetary Sciences*, *27*(1), 385–415. https://doi.org/10.1146/annurev.earth.27.1.385

Michalski, J., & Niles, P. B. (2012). Atmospheric origin of Martian interior layered deposits: Links to climate change and the global sulfur cycle. *Geology*, *40*(5), 419–422. https://doi.org/10.1130/g32971.1

Michalski, J. R., & Bleacher, J. E. (2013). Supervolcanoes within an ancient volcanic province in Arabia Terra, Mars. *Nature*, *502*(7469), 47–52. https://doi.org/10.1038/nature12482

Michalski, J. R., Cuadros, J., Niles, P. B., Parnell, J., Rogers, A. D., & Wright, S. P. (2013). Groundwater activity on Mars and implications for a deep biosphere. *Nature Geoscience*, *6*(2), 133–138. https://doi.org/10.1038/ngeo1706

Michalski, J. R., Glotch, T. D., Rogers, A. D., Niles, P. B., Cuadros, J., Ashley, J. W., & Johnson, S. S. (2019). The geology and astrobiology of McLaughlin Crater, Mars: An ancient lacustrine basin containing turbidites, mudstones, and serpentinites. *Journal of Geophysical Research*, *124*(4), 910–940. https://doi.org/10.1029/2018JE005796

Molina, A., López, I., Prieto-Ballesteros, O., Fernández-Remolar, D., de Pablo, M. Á., & Gómez, F. (2017). Coogoon Valles, western Arabia Terra: Hydrological evolution of a complex Martian channel system. *Icarus*, *293*, 27–44. https://doi.org/10.1016/j.icarus.2017.04.002

Morgan, G. A., Campbell, B. A., Carter, L. M., & Plaut, J. J. (2015). Evidence for the episodic erosion of the Medusae Fossae Formation preserved within the youngest volcanic province on Mars. *Geophysical Research Letters*, *42*(18), 7336–7342. https://doi.org/10.1002/2015GL065017

Murana, A. (2018). Geology of Danielson Crater, Mars. *Journal of Maps*, *14*(2), 161–172. https://doi.org/10.1080/17445647.2018.1443029

Murchie, S. L., Mustard, J. F., Ehlmann, B. L., Milliken, R. E., Bishop, J. L., McKeown, N. K., & Bibring, J. P. (2009). A synthesis of Martian aqueous mineralogy after 1 Mars year of observations from the Mars Reconnaissance Orbiter. *Journal of Geophysical Research*, *114*(E2). https://doi.org/10.1029/2009je003342

Neukum, G., & Jaumann, R. (2004). HRSC: The high resolution stereo camera of Mars Express. In *Mars express: The scientific payload* (Vol. 1240, pp. 17–35).

Neukum, G., Basilevsky, A. T., Kneissl, T., Chapman, M. G., Van Gasselt, S., Michael, G., et al. (2010). The geologic evolution of Mars: Episodicity of resurfacing events and ages from cratering analysis of image data and correlation with radiometric ages of Martian meteorites. *Earth and Planetary Science Letters*, *294*(3–4), 204–222. https://doi.org/10.1016/j.epsl.2009.09.006

Newsom, H. E., Barber, C. A., Hare, T. M., Schelble, R. T., Sutherland, V. A., & Feldman, W. C. (2003). Paleolakes and impact basins in southern Arabia Terra, including Meridiani Planum: Implications for the formation of hematite deposits on Mars. *Journal of Geophysical Research*, *108*(E12). https://doi.org/10.1029/2002JE001993

Niles, P. B., & Michalski, J. (2009). Meridiani Planum sediments on Mars formed through weathering in massive ice deposits. *Nature Geoscience*, *2*(3), 215–220. https://doi.org/10.1038/ngeo438

Noe Dobrea, E. Z., Michalski, J., & Swayze, G. (2011). Aqueous mineralogy and stratigraphy at and around the proposed Mawrth Vallis MSL Landing Site: New insights into the aqueous history of the region. *MARS*, *6*, 32–46. https://doi.org/10.1555/mars.2011.0003

Noe Dobrea, E. Z., Wray, J. J., Calef, F. J., III, Parker, T. J., & Murchie, S. L. (2012). Hydrated minerals on Endeavour Crater's rim and interior, and surrounding plains: New insights from CRISM data. *Geophysical Research Letters*, *39*, L23201. https://doi.org/10.1029/2012GL053180

Noel, A., Bishop, J. L., Al-Samir, M., Gross, C., Flahaut, J., McGuire, P. C., et al. (2015). Mineralogy, morphology and stratigraphy of the light-toned interior layered deposits at Juventae Chasma. *Icarus*, *251*, 315–331. https://doi.org/10.1016/j.icarus.2017.11.00610.1016/j.icarus.2014.09.033

Oehler, D. Z., & Allen, C. C. (2010). Evidence for pervasive mud volcanism in Acidalia Planitia, Mars. *Icarus*, *208*(2), 636–657. https://doi.org/10.1016/j.icarus.2010.03.031

Okubo, C. H., Lewis, K. W., McEwen, A. S., & Kirk, R. L. (2008). Relative age of interior layered deposits in southwest Candor Chasma based on high-resolution structural mapping. *Journal of Geophysical Research*, *113*(E12). https://doi.org/10.1029/2008JE003181

Pangaea Scientific (2011). Supported by Canada Centre for Remote Sensing, Natural Resources Canada. Orion: Orientation Hunter [computer software].

Pondrelli, M., Rossi, A. P., Ori, G. G., Van Gasselt, S., Praeg, D., & Ceramicola, S. (2011). Mud volcanoes in the geologic record of Mars: The case of Firsoff crater. *Earth and Planetary Science Letters*, *304*(3–4), 511–519. https://doi.org/10.1016/j.epsl.2011.02.027

Pondrelli, M., Rossi, A. P., Le Deit, L., Fueten, F., van Gasselt, S., Glamoclija, M., et al. (2015). Equatorial layered deposits in Arabia Terra, Mars: Facies and process variability. *Bulletin*, *127*(7–8), 1064–1089. https://doi.org/10.1130/b31225.1

Pondrelli, M., Rossi, A. P., Le Deit, L., Schmidt, G. W., Pozzobon, R., Hauber, E., & Salese, F. (2019). Groundwater control and process variability on the equatorial layered deposits of Kotido crater, Mars. *Journal of Geophysical Research: Planets*, *124*. https://doi.org/10.1029/2018je005656

Poulet, F., Arvidson, R. E., Gomez, C., Morris, R. V., Bibring, J. P., Langevin, Y., et al. (2008). Mineralogy of Terra Meridiani and western Arabia Terra from OMEGA/MEx and implications for their formation. *Icarus*, *195*, 106–130. https://doi.org/10.1016/j.icarus.2007.11.031

Pozzobon, R., Mazzarini, F., Massironi, M., Rossi, A. P., Pondrelli, M., Cremonese, G., & Marinangeli, L. (2019). Fluids mobilization in Arabia Terra, Mars: Depth of pressurized reservoir from mounds self-similar clustering. *Icarus*, *321*, 938–959. https://doi.org/10.1016/j.icarus.2018.12.023

Quantin-Nataf, C., Carter, J., Mandon, L., Thollot, P., Balme, M., Volat, M., et al. (2021). Oxia Planum: The landing site for the ExoMars "Rosalind Franklin" rover mission: Geological context and prelanding interpretation. *Astrobiology*, *21*(3), 345–366. https://doi.org/10.1089/ast.2019.2191

Rodriguez, J. A. P., Fairén, A. G., Tanaka, K. L., Zarroca, M., Linares, R., Platz, T., et al. (2016). Tsunami waves extensively resurfaced the shorelines of an early Martian ocean. *Scientific Reports*, *6*(1), 1–14. https://doi.org/10.1016/j.pss.2015.12.009

Rossi, A. P., Neukum, G., Pondrelli, M., Van Gasselt, S., Zegers, T., Hauber, E., et al. (2008). Large-scale spring deposits on Mars? *Journal of Geophysical Research*, *113*, E08016. https://doi.org/10.1029/2007je003062

Salese, F., Pondrelli, M., Neeseman, A., Schmidt, G., & Ori, G. G. (2019). Geological evidence of planet-wide groundwater system on Mars. *Journal of Geophysical Research: Planets*, *124*(2), 374–395. https://doi.org/10.1029/2018JE005802

Salese, F., Ansan, V., Mangold, N., Carter, J., Ody, A., Poulet, F., & Ori, G. G. (2016). A sedimentary origin for intercrater plains north of the Hellas basin: Implications for climate conditions and erosion rates on early Mars. *Journal of Geophysical Research: Planets*, *121*(11), 2239–2267. https://doi.org/10.1002/2016JE005039

Sarkar, R., Edgett, K. S., Singh, P., & Porwal, A. (2018). The light-toned stratified sedimentary rock exposures in western Juventae Chasma, Mars, in context. *Icarus*, *312*, 7–35. https://doi.org/10.1016/j.icarus.2018.04.010

Schmidt, G. (2021). Spreadsheets of layer measurements and calculations in Arabia Terra. https://doi.org/10.5281/zenodo.5150395

Schmidt, G., Fueten, F., Stesky, R., Flahuat, J., & Hauber, E. (2018). Geology of Hebes Chasma, Mars: 1. Structure, stratigraphy, and mineralogy of the interior layered deposits. *Journal of Geophysical Research: Planets*, *123*, 2893–2919. https://doi.org/10.1029/2018JE005658

Sefton-Nash, E., Catling, D. C., Wood, S. E., Grindrod, P. M., & Teanby, N. A. (2012). Topographic, spectral and thermal inertia analysis of interior layered deposits in Iani Chaos, Mars. *Icarus*, *221*(1), 20–42. https://doi.org/10.1016/j.icarus.2012.06.036

Shean, D. E., Alexandrov, O., Moratto, Z. M., Smith, B. E., Joughin, I. R., Porter, C., & Morin, P. (2016). An automated, open-source pipeline for mass production of digital elevation models (DEMs) from very-high-resolution commercial stereo satellite imagery. *ISPRS Journal of Photogrammetry and Remote Sensing*, *116*, 101–117. https://doi.org/10.1016/j.isprsjprs.2016.03.012

Silvestro, S., Pacifici, A., Salese, F., Vaz, D. A., Neesemann, A., Tirsch, D., et al. (2021). Periodic bedrock ridges at the ExoMars 2022 landing site: Evidence for a changing wind regime. *Geophysical Research Letters*, *48*(4), e2020GL091651. https://doi.org/10.1029/2020GL091651

Smith, D. E., Zuber, M. T., Frey, H. V., Garvin, J. B., Head, J. W., Muhleman, D. O., et al. (2001). Mars orbiter laser altimeter: Experiment summary after the first year of global mapping of Mars. *Journal of Geophysical Research*, *106*(E10), 23689–23722. https://doi.org/10.1029/2000JE001364

Smith, D. E., Zuber, M. T., Solomon, S. C., Phillips, R. J., Head, J. W., Garvin, J. B., et al. (1999). The global topography of Mars and implications for surface evolution. *Science*, *284*(5419), 1495–1503. https://doi.org/10.1126/science.284.5419.1495

Sowe, M., Jaumann, R., & Neukum, G. (2011). A comparative study of interior layered deposits on Mars. *Geological Society, London, Special Publications*, *356*(1), 281–300. https://doi.org/10.1144/SP356.14

Tanaka, K., & Platz, T. (2011). Plateau geology south of Valles Marineris, Mars: Implications for canyon formational history. In *EPSC-DPS joint meeting 2011* (Vol. 2011, p. 269)

Tanaka, K. L., Skinner, J. A., Jr, Dohm, J. M., Irwin, R. P., III, Kolb, E. J., Fortezzo, C. M., et al. (2014). Geologic map of Mars: U.S. *Geological Survey Scientific Investigations Mapscale 1:20,000*, *3292*, 43. https://doi.org/10.3133/sim3292

Thomson, B. J., Bridges, N. T., Milliken, R., Baldridge, A., Hook, S. J., Crowley, J. K., et al. (2011). Constraints on the origin and evolution of the layered mound in Gale Crater, Mars using Mars Reconnaissance Orbiter data. *Icarus*, *214*(2), 413–432. https://doi.org/10.1016/j.icarus.2011.05.002

U.S. Geological Survey (1973). Mars chart, MC-11, Oxia Palus Quadrangle. *Open-File Report*, 73–330. https://doi.org/10.3133/ofr73330

Vago, J., Witasse, O., Svedhem, H., Baglioni, P., Haldemann, A., Gianfiglio, G., et al. (2015). ESA ExoMars program: The next step in exploring Mars. *Solar System Research*, *49*(7), 518–528. https://doi.org/10.1134/S0038094615070199

Vago, J. L., Westall, F., Coates, A. J., Jaumann, R., Korablev, O., Ciarletti, V., et al. (2017). Habitability on early Mars and the search for biosignatures with the ExoMars Rover. *Astrobiology*, *17*(6–7), 471–510. https://doi.org/10.1089/ast.2016.1533

Webb, V. E. (2004). Putative shorelines in northern Arabia Terra, Mars. *Journal of Geophysical Research*, *109*(E9). https://doi.org/10.1029/2003JE002205

Weitz, C. M., Milliken, R. E., Grant, J. A., McEwen, A. S., Williams, R. M. E., Bishop, J. L., & Thomson, B. J. (2010). Mars Reconnaissance Orbiter observations of light-toned layered deposits and associated fluvial landforms on the plateaus adjacent to Valles Marineris. *Icarus*, *205*(1), 73–102. https://doi.org/10.1016/j.icarus.2009.04.017

Werner, S. C. (2005). *Major aspects of the chronostratigraphy and geologic evolutionary history of Mars*. Cuvillier Verlag.

Wharton, R. A., Crosby, J. M., McKay, C. P., & Rice, J. W. (1995). Paleolakes on Mars. *Journal of Paleolimnology*, *13*(3), 267–283. https://doi.org/10.1007/BF00682769

Whelley, P., Novak, A. M., Richardson, J., Bleacher, J., Mach, K., & Smith, R. N. (2021). Stratigraphic evidence for early Martian explosive volcanism in Arabia Terra. *Geophysical Research Letters*, *48*. https://doi.org/10.1029/2021GL094109

Wiseman, S. M., Arvidson, R. E., Morris, R. V., Poulet, F., Andrews-Hanna, J. C., Bishop, J. L. (2010). Spectral and stratigraphic mapping of hydrated sulfate and phyllosilicate-bearing deposits in northern Sinus Meridiani, Mars. *Journal of Geophysical Research*, *115*(E7). https://doi.org/10.1029/2009JE003354

Wray, J. J., Ehlmann, B. L., Squyres, S. W., Mustard, J. F., & Kirk, R. L. (2008). Compositional stratigraphy of clay-bearing layered deposits at Mawrth Vallis, Mars. *Geophysical Research Letters*, *35*(12). https://doi.org/10.1029/2008GL034385

Wray, J. J., Milliken, R. E., Dundas, C. M., Swayze, G. A., Andrews-Hanna, J. C., Baldridge, A. M., et al. (2011). Columbus crater and other possible groundwater-fed paleolakes of Terra Sirenum, Mars. *Journal of Geophysical Research 116*(E1). https://doi.org/10.1029/2010JE003694

Zabrusky, K., Andrews-Hanna, J. C., & Wiseman, S. M. (2012). Reconstructing the distribution and depositional history of the sedimentary deposits of Arabia Terra, Mars. *Icarus*, *220*(2), 311–330. https://doi.org/10.1016/j.icarus.2012.05.007

Zuber, M. T., Solomon, S. C., Phillips, R. J., Smith, D. E., Tyler, G. L., Aharonson, O., et al. (2000). Internal structure and early thermal evolution of Mars from Mars global surveyor topography and gravity. *Science*, *287*(5459), 1788–1793. https://doi.org/10.1126/science.287.5459.1788